repiSalud
Repositorio Institucional en Salud

This is the peer reviewed version of the following article:

Garcia-Redondo, A. B., Esteban, V., Briones, A. M., Diaz Del Campo, L. S., Gonzalez-Amor, M., Mendez-Barbero, N., . . . Salaices, M. (2018). Regulator of calcineurin 1 modulates vascular contractility and stiffness through the upregulation of COX-2-derived prostanoids. *Pharmacological Research, 133*, 236-249. doi:10.1016/j.phrs.2018.01.001

which has been published in final form at: https://doi.org/10.1016/j.phrs.2018.01.001

Regulator of calcineurin 1 modulates vascular contractility and stiffness through the upregulation of COX-2-derived prostanoids.

[1,2]Ana B. García-Redondo, [3,4]Vanesa Esteban, [1,2*]Ana M. Briones, [1]Lucía S. Díaz del Campo, [3]Nerea Méndez-Barbero, [2,5]Miguel R. Campanero, [2,3]Juan M. Redondo, [1,2*]Mercedes Salaices.

[1]Departamento de Farmacología, Facultad de Medicina, Universidad Autónoma de Madrid, Instituto de Investigación Hospital Universitario La Paz (IdiPAZ), Madrid, Spain. [2]CIBER de Enfermedades Cardiovasculares; [3]Gene Regulation in Cardiovascular Remodeling and Inflammation Group, Centro Nacional de Investigaciones Cardiovasculares (CNIC), Madrid, Spain. [4]Departamento de Inmunología, Instituto de Investigación Fundación Jiménez Díaz, Madrid, Spain. [5]Departmento de Biología del Cáncer, Instituto de Investigaciones Biomédicas Alberto Sols, CSIC-UAM, Madrid, Spain

Ana B. Garcia-Redondo and Vanesa Esteban contributed equally to this paper.

Corresponding authors:

*Mercedes Salaices: mercedes.salaices@uam.es

Departamento de Farmacología. Universidad Autónoma de Madrid

Arzobispo Morcillo 4, 28029 Madrid, Spain

Phone: 34914975378. Fax: 34914975380

*Ana M. Briones: ana.briones@uam.es

Departamento de Farmacología. Universidad Autónoma de Madrid

Arzobispo Morcillo 4, 28029 Madrid, Spain

Phone: 34914975399. Fax: 34914975380

Running title: Rcan1/COX-2 and vascular contractility/stiffness

Abstract

Cyclooxygenase-2 (COX-2) derived-prostanoids participate in the altered vascular function and mechanical properties in cardiovascular diseases. We investigated whether regulator of calcineurin 1 (Rcan1) participates in vascular contractility and stiffness through the regulation of COX-2. For this, wild type (*Rcan1*$^{+/+}$) and *Rcan1*-deficient (*Rcan1*$^{-/-}$) mice untreated or treated with the COX-2 inhibitor rofecoxib were used. Vascular function and structure were analysed by myography. COX-2 and phospo-p65 expression were studied by western blotting and immunohistochemistry and TXA_2 production by ELISA. We found that *Rcan1* deficiency increases COX-2 and IL-6 expression and NF-κB activation in arteries and vascular smooth muscle cells (VSMC). Adenoviral-mediated re-expression of Rcan1.4 in *Rcan1*$^{-/-}$ VSMC normalized COX-2 expression. Phenylephrine-induced vasoconstrictor responses were greater in aorta from *Rcan1*$^{-/-}$ compared to *Rcan1*$^{+/+}$ mice. This increased response were diminished by etoricoxib, furegrelate, SQ29548, cyclosporine A and parthenolide, inhibitors of COX-2, TXA_2 synthase, TP receptors, calcineurin and NF-κB, respectively. Endothelial removal and NOS inhibition increased phenylephrine responses only in *Rcan1*$^{+/+}$ mice. TXA_2 levels were greater in *Rcan1*$^{-/-}$ mice. In mesenteric resistance arteries, vascular function and structure were similar in both groups of mice; however, vessels from *Rcan1*$^{-/-}$ mice displayed an increase in vascular stiffness that was diminished by rofecoxib. In conclusion, our results suggest that Rcan1 might act as endogenous negative modulator of COX-2 expression and activity by inhibiting calcineurin and NF-kB pathways to maintain normal vascular stiffness and contractility. Our results uncover a new role for Rcan1 in vascular contractility and mechanical properties.

Key words: Rcan1; COX-2; vascular function and stiffness

Abbreviations

Cn, calcineurin; COX-2, cyclooxygenase-2; KHS, Krebs Henseleit Solution; NO, nitric oxide; *Rcan1*, Regulator of calcineurin 1; ROS, reactive oxygen species; MRA, mesenteric resistance arteries; TXA_2, thromboxane A_2; VSMC, vascular smooth muscle cells.

Introduction

Prostanoids synthesized by cyclooxygenases (COX), the constitutive COX-1 or the inducible COX-2, are critical modulators of vascular tone in physiological and pathological conditions. COX-2 is induced by inflammatory stimuli and other factors important for cardiovascular diseases such as angiotensin II or endothelin-1 [1-4] and it is increased in pathological conditions [5-7]. Of note, increased production of vasoconstrictor substances and COX-2 is responsible for the greater vasoconstrictor responses, endothelial dysfunction and increased vascular stiffness observed in different pathologies such as hypertension both in animal models [2, 8-13] and in humans [14, 15].

Calcineurin (Cn) is a calcium/calmodulin dependent serine/threonine protein phosphatase that plays a key role in many cellular processes [16]. The interaction of Cn with the nuclear factor of activated T cell (NFAT) c1-c4 family triggers their rapid translocation to the nucleus where they become transcriptionally active [17]. NFATs were originally identified in lymphoid cells, but they play a critical role in the regulation of physiological functions of many different cells, including vascular smooth muscle cells (VSMC) and endothelial cells [18-20]. Cn inhibitors are widely used drugs that ameliorate organ rejection. However, they produce cardiovascular side effects such as hypertension through modulation of NO and prostanoids pathways. Thus, hypertension in cyclosporine-treated cardiac transplant recipients is associated with decreased prostaglandin levels and increased thromboxane A_2 synthesis [21]. Although many of the effects of Cn inhibitors can be explained by inhibition of the Cn/NFAT pathway, it has also been described that cyclosporine A toxicity is at least partly independent of this pathway [22, 23]. Both Cn/NFAT and the nuclear transcription factor NF-κB are well known modulators of the expression of a number of enzymes involved in the production of mediators that participate in the control of vascular tone and structure. Among the best characterized are eNOS [24, 25], COX-2 [26-30] and some sources of reactive oxygen species (ROS) such as the NADPH Oxidase [31]. Interestingly, a crosstalk between NFAT and NF-κB in the control of COX-2 expression has been suggested in human epithelial cells [32].

Regulator of calcineurin 1 (Rcan1) was first identified as a negative regulator of Cn activity [33]. However, increasing evidence indicate that Rcan1 can also increase [34, 35] or not affect [36, 37] Cn activity, suggesting that the effects of Rcan1 on Cn may be

context-dependent. In addition, novel evidence point to its role in triggering the stabilization of the inhibitor of NF-κB (Iκ-B) therefore attenuating NF–κB transcriptional activation [38-41]. The fact that Rcan1 has been implicated in the development of several inflammatory diseases, point to the importance of Rcan1 as a potent negative regulator of inflammation [38-40, 42, 43]. However, at cardiovascular level, the role of Rcan1 is still far from being totally understood. Thus, Rcan1 has been described as inhibitor [35, 44] and as inductor [35] of cardiac hypertrophy depending on the stimuli. In addition, we previously reported that *Rcan1*-deficient (*Rcan1*$^{-/-}$) mice were resistant to angiotensin II-induced aneurysms, neointima formation and atherosclerosis [36, 37]. However, knowledge about its role in vascular contractility is limited and no evidence on how *Rcan1* participates in vascular structure and mechanical properties has been provided. The aim of the present study was to shed light on the role of Rcan1 and its possible downstream pathways namely Cn, NF-kB and COX-2 in vascular contractility and structure.

Methods

Animal experimental design

All experimental procedures were approved by the Animal Care and Use Committee of Centro Nacional de Investigaciones Cardiovasculares (CNIC), Universidad Autónoma de Madrid and by the Madrid regional authorities (ref. PROEX 345/14), and conformed to European Union guidelines for the care and experimental use of animals. The study was conducted in accordance with the National Institutes of Health (NIH) Guide for the Care and Use of Laboratory Animals (NIH Publication No. 85-23, revised 1996) and the Spanish Policy for Animal Protection RD53/2013, which meets the European Union Directive 2010/63/UE on the protection of animals used for experimental and other scientific purposes. The studies are also in accordance with the ARRIVE guidelines for reporting experiments involving animals [45]. A total of 102 mice were used.

Three-month-old male *Rcan1*$^{-/-}$ and *Rcan1*$^{+/+}$ mice in C57BL6 genetic background as previously described [46] were used. Animals (approximate weight 25 gr) were breed at the Animal Care Facility of the CNIC. *Rcan1*$^{-/-}$ and *Rcan1*$^{+/+}$ matched controls were produced by crossing the *Rcan1* heterozygous mutant line. Some *Rcan1*$^{-/-}$ mice were

treated with the selective COX-2 inhibitor rofecoxib (10 mg·kg^{-1}·day^{-1} i.p., 14 days) or vehicle (0.5% carboxymethylcellulose, 0.025% tween 20, 14 days), as previously described [13]. Animals were housed under controlled conditions at 25°C in a 12 h light/dark cycle with ad libitum access to water and food. Overall mouse health was assessed by daily inspection for signs of discomfort, weight loss, or changes in behaviour, mobility, and feeding or drinking habits. All mice were genotyped by PCR of tail samples using the following primers: *Rcan1*, 5′-GGTGGTCCACGTGTGTGAGA-3′, 5′ -ACGTGAACAAAGGCTGGTCCT-3, and 5′-ATTCGCAGCGCATCGCCTTCTATCGCC-3′. Blood pressure was measured by tail-cuff plethysmography. For this, animals were trained for one week prior to final blood pressure measurements by blinded observers that were unaware of the vascular experiments. Measurements were done always at the same time of the day from 8-10 am. 5 individual observations were performed and averaged for each animal. For cell culture procedures and vascular reactivity experiments, mice used were sacrificed by CO_2 inhalation and exsanguination.

Tissue preparation

Aorta and first-order branches of the mesenteric artery were dissected free of fat and connective tissue and placed in cold Krebs Henseleit Solution (KHS) (115 mM NaCl, 25 mM $NaHCO_3$, 4.7 mM KCl, 1.2 mM $MgSO_4$.7H2O, 2.5 mM $CaCl_2$, 1.2 mM KH2PO_4, 11.1 mM glucose, and 0.01 mM Na_2EDTA) bubbled with a 95% O_2-5% CO_2 mixture. Analysis of vascular function, structure and mechanics was done on the same day. For immunohistochemistry or immunofluorescence, aortic segments were fixed in 4% paraformaldehyde. Other vascular segments were immediately frozen in liquid nitrogen and kept at –70ºC until further processing for gene expression and western blot studies.

Plasma samples

Blood samples were collected in tubes containing EDTA (Deltalab), inverted gently from 4 to 6 times and placed in ice. After that, blood sample were centrifuged at 1500 x g for 15 minutes. Plasma samples were frozen at -70ºC.

Vascular function

Thoracic aorta and mesenteric resistance arteries (MRA) from *Rcan1*$^{-/-}$ and *Rcan1*$^{+/+}$ mice were dissected and segments, 2 mm in length, were mounted in a small-vessel chamber myograph for measurement of isometric tension according to the method described previously [12]. After a 30-min equilibration period in oxygenated KHS at 37°C and pH 7.4, segments were stretched to their optimal lumen diameter for active tension development. Segments were washed with KHS and left to equilibrate for 30 min; then, contractility was tested by an initial exposure to a high-K^+ solution (120 mM, KCl). The presence of endothelium was determined by the ability of 10 μM acetylcholine to induce relaxation in arteries precontracted with phenylephrine to achieve a contractile response of approximately 50% of K^+-KHS contraction. Afterwards, concentration-response curves to acetylcholine (1 nM-10 μM) in phenylephrine precontracted arteries or to phenylephrine (1 nM-30 μM) were performed. The role of Cn or NF-κB signalling pathways on phenylephrine-induced contraction was analysed in arteries incubated with the Cn inhibitor cyclosporine A (200 ng/ml) or the NF-κB inhibitor parthenolide (1 μM), which were added when the aorta was removed from the animal. The COX-2 inhibitor etoricoxib (1 μM), the TXA synthase inhibitor furegrelate (1 μM), the TP inhibitor SQ 29548 (1 μM), the NOS inhibitor *N*-nitro-L-arginine methyl ester (L-NAME, 100 μM), or the antioxidant tiron (1 mM) were added 30 min before phenylephrine. Vasoconstrictor responses were expressed as a percentage of the contraction to KCl and vasodilator responses were expressed as a percentage of the previous contraction to phenylephrine.

In another set of experiments, endothelium removal was performed. For this, a hair was introduced into the vessel lumen and used it to mechanically remove the endothelial layer. Endothelium removal was assessed by the inability of 10 μM acetylcholine to produce vasodilatation.

Pressure myography

The structural and mechanical properties of mesenteric resistance arteries (MRA) were studied with a pressure myograph (Danish Myo Tech, Model P100, J.P. Trading I/S, Aarhus, Denmark). Vessels were placed on two glass microcannula and secured with surgical nylon suture. After any small branches were tied off, vessel length was adjusted so that the vessel walls were parallel without stretch. Intraluminal pressure was then raised to 120 mmHg, and the artery was unbuckled by adjusting the cannula. The segment

was then set to a pressure of 45 mmHg and allowed to equilibrate for 60 min at 37°C in calcium-free KHS ($0Ca^{2+;}$ omitting calcium and adding 1 mM EGTA) extravascular and intravascularly perfused, gassed with a mixture of 95% O_2 and 5% CO_2. Intraluminal pressure was then reduced to 3 mmHg. A pressure-diameter curve was obtained by increasing intraluminal pressure in 20 mmHg steps from 3 to 120 mmHg. Finally, the artery was set to 45 mmHg in $0Ca^{2+}$-KHS and then pressure-fixed with 4% paraformaldehyde in 0.2 M phosphate buffer, pH 7.2-7.4 at 37°C for 60 min and kept in 4% paraformaldehyde at 4°C for confocal microscopy studies.

Internal and external diameters were continuously measured under passive conditions (D_{i0Ca}, D_{e0Ca}) for 2 min at each intraluminal pressure. The final value used was the mean of the measurements taken during the last 30 s when the measurements reached a steady state. From internal and external diameter measurements in passive conditions the following structural and mechanical parameters were calculated:

Wall thickness (WT) = $(D_{e0Ca} - D_{i0Ca})/2$

Cross-sectional area (CSA) = $(\pi/4) \times (D_{e0Ca}^2 - D_{i\,Ca}^2)$

Wall:lumen = $(D_{e0Ca} - D_{i0Ca})/2D_{i0Ca}$

Incremental distensibility represents the percentage of change in the arterial internal diameter for each mmHg change in intraluminal pressure and was calculated according to the formula:

Incremental distensibility = $\Delta D_{i0Ca}/(D_{i0Ca} \times \Delta P) \times 100$.

Circumferential wall strain (ε) = $(D_{i0Ca} - D_{00Ca})/D_{00Ca}$, where D_{00Ca} is the internal diameter at 3 mmHg and D_{i0Ca} is the observed internal diameter for a given intravascular pressure both measured in $0Ca^{2+}$ medium.

Circumferential wall stress (σ) = $(P \times D_{i0Ca})/(2WT)$, where P is the intraluminal pressure (1 mmHg = 1.334×10^3 dynes·cm^{-2}) and WT is wall thickness at each intraluminal pressure in $0Ca^{2+}$-KHS.

Arterial stiffness independent of geometry is determined by the Young's elastic modulus (E =stress/strain). The stress-strain relationship is non-linear; therefore, it is more appropriate to obtain a tangential or incremental elastic modulus (E_{inc}) by determining the

slope of the stress-strain curve ($E_{inc} = \delta\sigma/\delta\varepsilon$). E_{inc} was obtained by fitting the stress-strain data from each animal to an exponential curve using the equation: $\sigma = \sigma_{orig} e^{\beta\varepsilon}$, where σ_{orig} is the stress at the original diameter (diameter at 3 mmHg). Taking derivatives on the equation presented earlier, we see that $E_{inc} = \beta\sigma$. For a given σ-value, E_{inc} is directly proportional to β. An increase in β implies an increase in E_{inc}, which means an increase in stiffness.

Determination of aortic structure and elasticity

Aortic rings elasticity was determined using a wire myograph (Danish Myo Tech) as previously described [47] with some modifications. After a 30-min equilibration period in oxygenated $0Ca^{2+}$-KHS to avoid active constriction, passive vascular properties were assessed by exposure to stepwise increases in stretching (200 μm steps, 1 min each) while recording the developed force. This approach calculates vessel elasticity independently of smooth muscle tone but it does not exclude the influence of vascular remodeling.

The vessels were assumed to be cylinders, the length of which did not vary with changes in radius. Since the vessels were found to be flat between the wires, the internal circumference (L) and hence diameter of each vessel segment at each corresponding pressure were calculated using the equation below where *d* is the diameter of the mounting wires and *s* is the separation of the wires from each other's inner surface.

$$L = (\pi + 2) \times d + 2 \times s$$

The circumferential wall force per unit length is the passive wall tension T and was calculated from the following equation which took into account the fact that the forces produced by a ring are equal to twice the force which would have been produced by an equivalent aortic strip, where *F* is the force exerted by the vessel on the tension transducer and *g* is the vessel length:

$$T = F / 2 \times g$$

Effective transmural pressure P was calculated from Laplace's equation where *L* is the internal circumference corresponding to the wall tension:

$$P = 2 \times \pi \times T / L$$

Assuming that the wall cross-sectional area remains practically constant through a range of intraluminal pressures, this parameter was calculated from individual histological hematoxylin-eosin stained transverse sections once the stretching curve was performed. External diameter (De) was then extrapolated from the formula:

$CSA = \pi/4 \times (De^2 - Di^2)$

where Di is the internal diameter calculated from internal circumference at each pressure:

$Di = L / \pi$

Wall thickness was then calculated as stated above.

Organization of internal elastic lamina

The elastin organization within the internal elastic lamina was studied in segments of MRA, using fluorescence confocal microscopy based on the autofluorescent properties of elastin (excitation wavelength 488 nm and emission wavelength 500-560 nm), as previously described [52]. Briefly, the experiments were performed in intact pressure-fixed segments with a Leica TCS SP2 confocal system (Leica Microsystems, Wetzlar, Germany). Serial optical sections from the adventitia to the lumen (z step = 0.5 μm) were captured with a X40 oil objective (Zoom 4), using the 488 nm line of the confocal microscope. A minimum of two stacks of images of different regions were captured in each arterial segment. Quantitative analysis of the internal elastic lamina was performed with Metamorph Image Analysis Software, as previously described [48]. From each stack of serial images, individual projections of the internal elastic lamina were reconstructed, and total fenestrae number and mean fenestrae area were measured.

Cell culture

For isolation of VSMC, abdominal and thoracic aortas from *Rcan1*$^{-/-}$ and *Rcan1*$^{+/+}$ mice were dissected and processed as previously described [36]. Explants were not disturbed during the first days. After outgrowth of adherent cells, cultures were trypsinized and subcultured. All experiments were performed during passages 3–7. Before stimulation, cells were rendered quiescent for 48 h by incubation in serum-free medium. For *Rcan1* re-expression experiments, VSMCs were infected with adenoviruses expressing either GFP-tagged Rcan1.4 (Adeno-Rcan1) or GFP (Adeno-GFP; 1.6×10^8 pfu/ml). Infection

efficiency was monitored by flow cytometry (FACS Canto; BD) as previously described [36].

Immunoblot analysis

Protein extracts from VSMC or aortic segments were obtained using an ice-cold lysis buffer, separated under reducing conditions on SDS-polyacrylamide gels and transferred to nitrocellulose membranes as described [36].

Protein detection was performed with antibodies and dilutions as follows: anti-COX-2 (1:1000 Cayman, cat: 160126), anti-TXA synthase (1:1000 Cayman, cat: 160715), anti-phospo-p65 (1:2000 Cell Signaling, cat:3031), anti-α-tubulin (1:40,000 Sigma-Aldrich), anti-β-actin (1:100,000 Sigma Aldrich; cat:A3854), eNOS (1:500, BD, cat:610297), p-Akt (1:500, Cell Signalling, cat:9271S), anti-Rcan (1:500 Sigma, cat: D6694), anti-Can (1:250, Pharmigen, cat:65061A) and HRP-conjugated secondary antibodies. Immunocomplexes were detected with enhanced chemiluminescence (ECL) detection reagent (Millipore) and subjected to autoradiography (Hyperfilm ECL; Amersham). Signals on the immunoblot were quantified using ImageJ (v 1.45s). β-actin or α-tubulin were used as loading control.

RT and real-time PCR analysis

Total RNA was DNase-treated and reverse-transcribed as described [40]. Real-time quantitative RT-PCR was performed using TaqMan Gene Expression assays specific for mouse *Cox-2* (Mm00478374_m1), *Il-6* (Mm00446190_m1) *and Adr1* (Mm01328600_m1) or Syber probes: *Col1a2* (Fw: GTCCTAGTCGATGGCTGCTC, Rv: AGCACCACCAATGTCCAGAG), *Fn1* (Fw: ATGAGAAGCCTGGATCCCCT, Rv: GGAAGGGTAACCAGTTGGGG). Calculations were made from measurements of 2 replicates of each sample. The amount of target mRNA in samples was estimated by the 2CT relative quantification method using *Hprt1* (Mm00446968_m1) or *β2 microglobulin* (Fw: ACCCTGGTCTTTCTGGTGCTT, Rv: TAGCAGTTCAGTATGTTCGGCTT) for normalization.

Measurement of TXB_2 and PGE_2

The levels of the metabolite of TXA_2, TXB_2, were determined in the incubation medium using an enzyme immunoassay commercial kit following the manufacturer's instructions

(Cayman Chemical). For this, pooled mesenteric arteries (first and second order branches) from each mice were equilibrated in 300 µl of oxygenated KHS (37°C) for 30 min. Thereafter, to mimic the situation of the arteries mounted in the myograph, a phenylephrine concentration–response curve was performed keeping the same doses and times. At the end, the medium and the arteries were collected and frozen (-70°C) for TXB_2 and protein determination, respectively. TXB_2 values were measured and normalized per mg protein.

Plasma PGE_2 levels were determined using an enzyme immunoassay commercial kit following the manufacturer's instructions (Arbor Assays).

Measurement of NOx levels

After protein deproteinization with ethanol (1:2 v/v), plasma NOx (nitrite plus nitrate) levels were determined using a colorimetric commercial kit (Arbor Assays) following the manufacturer's instructions.

Immunohistochemistry

Paraffin-embedded sections were stained using standard histology procedures. Immunostaining was carried out in 3 µm thick tissue sections that were deparaffinised and antigen retrieved using the PT Link system (Dako Diagnósticos S.A, Barcelona, Spain) with Sodium Citrate Buffer (10 mmol/L) adjusted to pH=6. Endogenous peroxidase was blocked and aorta sections were incubated with the NF-kB p-p65 subunit antibody (1:500 Abcam, Cambrigde, UK) or COX-2 antibody (1:100 Santa Cruz Biotechnology, Inc) overnight at 4ºC. After washing, slides were treated with the corresponding anti-IgG biotinylated-conjugated secondary antibody (Amersham Bioscience) followed by the avidin-biotin-peroxidase complex, and 3,3'-diaminobenzidine as chromogen (Dako). Sections were counterstained with Carazzi's hematoxylin and mounted with DPX. The specificity was checked by omission of primary antibodies and use of non-immune sera. Images were obtained with the Nikon Eclipse E400 microscope, and analysed by Imagepro-plus (Media Cybernetics Inc. Rockville, MD, USA). All samples were evaluated in a blinded fashion. For each mouse, the mean score value was obtained by evaluating 4 different high-power fields (40X) per section.

Immunofluorescence

Paraffin-embedded sections were treated as described above. Aorta sections were blocked with FBS 5% and incubated with the anti-COX-1 (1:100, Abcam, Cambrigde, UK), anti-COX-2 (1:50, Santa Cruz Biotechnology, Inc), anti-Calcineurin A (1:50, BD Pharmigen) or anti-Rcan1 (Sigma-Aldrich) antibodies overnight at 4ºC. After washing, slides were treated with the corresponding fluorescent secondary antibody (Amersham Bioscience). Sections were counterstained with DAPI (Sigma) and mounted with Prolong (Thermofisher). The specificity was checked by omission of primary antibodies and use of non-immune sera. Images were obtained with a Leica TCS SP2 confocal system (Leica Microsystems, Wetzlar, Germany). Serial optical sections (z step = 1 μm) were captured with a X20 or X40 oil objective and analysed by Imagepro-plus (Media Cybernetics Inc. Rockville, MD, USA). All samples were evaluated in a blinded fashion.

Statistical analysis

All data are expressed as means ± s.e.m. For studies, we performed a minimum of 5 independent experiments. For statistical analysis, we used normalized data to reduce variability of baseline between independent experiments in protein and gene expression studies. Data were normalized as fold increase over $Rcan1^{+/+}$ mean. Group size for parametric testing was at least n = 5, regardless of any statistical power analysis. Student's t test, Mann-Whitney or one- or two-way ANOVA and Bonferroni's post-hoc tests were calculated using GraphPad Prism 5 software (GraphPad Software Inc., San Diego, CA). Statistical significance was assigned at $p < 0.05$.

Materials

The compounds used were supplied as follow: acetylcholine, phenylephrine, L-NAME, tiron, parthenolide, and furegrelate were from Sigma-Aldrich Co. (St Louis, MO, USA); SQ29548 (ICN Iberica); etoricoxib was a gift from Dr Godessart (Amirall Prodesfarma); Rofecoxib was from LKT Laboratories (St. Paul, MN, USA) and cyclosporin A was from Novartis.

Results

No changes in systolic blood pressure were found between both genotypes ($Rcan1^{+/+}$: 98.9 ± 3, n=5; $Rcan1^{-/-}$: 93.4 ± 3.6, n=5).

Rcan1 modulates vascular contractility

Contractile responses induced by KCl and endothelium-dependent relaxation induced by acetylcholine were similar in aorta and MRA from *Rcan1*$^{-/-}$ and *Rcan1*$^{+/+}$ mice (Figure 1A, Fig. S1A and Table 1). However, phenylephrine-induced contraction was greater in aortic segments from *Rcan1*$^{-/-}$ mice (Figure 1B, Table 1). This difference was not observed in MRA (Fig. S1B). mRNA levels of α1A-adrenoceptors were smaller in aorta from *Rcan1*$^{-/-}$ mice (Figure 1C).

Endothelium removal increased contractile responses to phenylephrine in aorta from *Rcan1*$^{+/+}$ but it did not modify phenylephrine responses in *Rcan1*$^{-/-}$ mice (Figure 1D) indicating that endothelial modulation of vasoconstrictor responses is lost in aorta from *Rcan1*$^{-/-}$ mice. Similarly, the NOS inhibitor L-NAME enhanced phenylephrine-induced contraction only in aorta from *Rcan1*$^{+/+}$ mice (Figure 1E). Aortic eNOS and pAkt expression (Figure 1F, Fig. S2) and plasma NOx levels (Fig. S1C) were similar in *Rcan1*$^{-/-}$ and *Rcan1*$^{+/+}$ mice these results suggest an unaltered NO production in arteries from *Rcan1*$^{-/-}$ mice. The antioxidant tiron inhibited the phenylephrine response only in aorta *Rcan1*$^{-/-}$ mice (Figure 1E) suggesting that oxidative stress might be implicated in the decreased NO availability observed in *Rcan1*$^{-/-}$

Rcan1 modulates vascular contractility through COX-2 dependent mechanisms

COX-2-derived vasoconstrictor prostanoids are also involved in the reduced NO effects and in the increased vasoconstrictor responses observed in pathological conditions [5, 8, 9,12]. COX-2 expression was observed in the three layers of the vascular wall in aorta from both genotypes (Figure 2A and Fig. S3A). Both *Cox-2* mRNA and protein levels were greater in aorta (Figure 2B,C and Fig. S2, S3A) and VSMCs (Figure 2D,E and Fig. S2) obtained from *Rcan1*$^{-/-}$ than in *Rcan1*$^{+/+}$ mice. Accordingly, adenoviral-mediated re-expression of Rcan1-4 in VSMCs from *Rcan1*$^{-/-}$ mice decreased COX-2 expression (Figure 2F and Fig. S2). COX-1 was also expressed in the three layers of the vascular wall and its mRNA levels were not affected by *Rcan1* deletion (Fig. S3B,C).

We then investigated the functional implication of the increased COX-2 expression observed in vessels from *Rcan1*$^{-/-}$ mice. The selective COX-2 inhibitor etoricoxib did not modify phenylephrine responses in aorta from *Rcan1*$^{+/+}$ mice but inhibited this response in *Rcan1*$^{-/-}$ mice (Figure 3A), suggesting that COX-2-derived contractile prostanoids are responsible for the increased phenylephrine responses in *Rcan1*$^{-/-}$mice. Similarly, the

TXA synthase inhibitor furegrelate (Figure 3A) and the TP antagonist SQ29548 (Figure 3B) decreased the phenylephrine-induced contraction only in aorta from *Rcan1*$^{-/-}$ mice, indicating that TXA_2 is a mayor contractile prostanoid involved in the hypercontractility to phenylephrine observed after *Rcan1* deletion. Accordingly, aortic segments from *Rcan1*$^{-/-}$ mice released greater levels of TXB_2 than *Rcan1*$^{+/+}$ mice (Figure 3C) without modification of TXA synthase protein levels (Figure 3D and Fig. S2). However, plasma levels of PGE_2 were similar in both genotypes (Fig. S3D).

Calcineurin and NF-κB pathways mediate the increased participation of COX-2-derived prostanoids on vasoconstrictor responses in Rcan1$^{-/-}$ *mice.*

Both NF-kB and Cn/NFAT can modulate COX-2 expression [26-29, 32] and previous reports have indicated that Rcan1 may regulate NF-kB via a Cn-dependent or independent mechanism [38,40]. Then we questioned the role of Cn and NF-κB in the altered vascular function observed in *Rcan1*$^{-/-}$mice. Cn, Rcan1 and COX-2 colocalized in the vascular wall (Fig. S4). We previously described that basal Cn enzymatic activity is unaltered in aortas from *Rcan1*$^{-/-}$mice [36]. However, phosphorylated p65 protein levels were greater both in VSMCs and aorta from *Rcan1*$^{-/-}$ compared to *Rcan1*$^{+/+}$ mice (Figure 4A, 4B and Fig. S2), suggesting higher NF-κB activity in *Rcan1*-deficient mice. In agreement, the levels of *Il-6*, an inflammatory cytokine closely related to NF-κB activation, were increased in aorta and VSMC from *Rcan1*$^{-/-}$ compared to *Rcan1*$^{+/+}$ mice (Figure 4C).

We then analysed the participation of Cn and NF-κB in the vascular contractile responses to phenylephrine. Neither the Cn inhibitor Cyclosporine A (CsA) (Figure 4D) or the NF-kB inhibitor parthenolide (Figure 4E) modified phenylephrine contraction in *Rcan1*$^{+/+}$ mice. However, a significant reduction of phenylephrine responses was observed for both inhibitors in *Rcan1*$^{-/-}$ mice (Figure. 4D,E), indicating the participation of both signalling pathways in the increased contractile response observed in *Rcan1*$^{-/-}$ mice. Moreover, incubation of CsA or parthenolide plus etoricoxib did not modify the effect of each drug alone on phenylephrine responses (Figure 4D,E), suggesting that Rcan1 modulates COX-2 activation through Cn and NF-kB pathways.

Rcan1 modulates vascular mechanical properties through COX-2 dependent mechanisms

We have recently demonstrated the key role of COX-2 in vascular stiffness [13]. Then, we analysed whether Rcan1 contributes to the structure and mechanics of the vascular

wall. Vessel and lumen diameter, wall:lumen ratio, wall thickness and cross-sectional area were similar in MRA from *Rcan1*$^{+/+}$ and *Rcan1*$^{-/-}$ mice (Figure 5A). However, media thickness and media CSA were smaller in aorta from *Rcan1*$^{-/-}$ compared to *Rcan1*$^{+/+}$ mice (Figure 5B).

MRA from *Rcan1*$^{-/-}$ mice showed a significant increase of vascular stiffness as shown by the leftward shift in the stress-strain curve and the increase in the elastic modulus β (Figure 6A). This effect might be due to a more compact elastin within the internal elastic lamina as shown by a tendency towards a smaller fenestra area and number that resulted in an increase area occupied by elastin (Figure 6B). Vessel elasticity in aorta was similar in aorta from *Rcan1*$^{-/-}$ and *Rcan1*$^{+/+}$ mice as shown by the similar tension-extension distance and 1/slope (Figure 6C). However, mRNA expression of collagen 1 but not fibronectin was increased in arteries from *Rcan1*$^{-/-}$ compared to *Rcan1*$^{+/+}$ mice (Figure 6D).

Rofecoxib treatment did not affect vascular structure neither in MRA or in aorta (Figure 5A,B). However, rofecoxib diminished vascular stiffness both in MRA and in aorta (Figure 6A,C). Intriguingly, rofecoxib treatment did not affect elastin structure in MRA (Figure 6B) but it decreased collagen mRNA levels without affecting fibronectin in aorta (Figure 6D).

Discussion

This study demonstrates that *Rcan1*-deficient mice exhibit increased vascular COX-2 expression and increased production of contractile prostanoids such as TXA_2, that contribute to the increased vasoconstrictor responses and stiffness observed in arteries from these mice.

Earlier studies demonstrated that during inflammation or vascular damage Rcan1 has a key role in modulating angiogenesis, migration and proliferation [49, 50]. In addition, we have previously described that Rcan1 plays a critical role in vascular remodelling associated with pathological states such as aneurysms, neointima formation and atherosclerosis [36, 37]. However, the contribution of Rcan1 to vascular tone and mechanical properties is poorly explored. In fact, to our knowledge, only other study performed in pressurized MRA has described decreased vascular contractile responses to phenylephrine [51]. We did not observe differences in blood pressure or contractile

responses in the wire-myograph mounted-MRA, however, *Rcan1* deletion increased vasoconstrictor responses to phenylephrine in aorta despite having a decrease in mRNA levels of α1A-adrenoceptors. The mechanisms responsible for this increased contractile response are also independent of altered contractile capacity of the SMC since KCl responses were similar in both groups. However, we found that endothelial removal or NOS inhibition increased vasoconstrictor responses to phenylephrine in wild type mice but not in *Rcan1*$^{-/-}$ mice, suggesting that the protective role of the endothelium is lost after *Rcan1* deletion. Interestingly, acetylcholine-induced relaxation, eNOS expression or Akt activation were similar in arteries from both genotypes, arguing against an altered NO production in arteries from *Rcan1*$^{-/-}$ mice. Mechanisms responsible for the loss of protective endothelium might include increased oxidative stress, since the antioxidant tiron inhibited phenylephrine responses only in vessels from *Rcan1*$^{-/-}$ mice. However, other mechanisms might be also involved.

Prostanoids are lipid mediators involved in the control of vascular tone, and increased COX-2 expression/activity participates of features of vascular damage, including hypercontractility, associated to pathologies like hypertension [8-10, 12]. Several reports have demonstrated a relationship between COX-2 and Rcan1. Thus, in human glioblastoma, endothelial cells and mouse primary astrocytes, Rcan1 deficiency induced an increase in COX-2 expression [38, 50, 52], observations now extended to VSMC. Thus, arteries and VSMC from *Rcan1*-deficient mice exhibited increased COX-2 expression and endothelial cells show a strong positive staining for the enzyme. Moreover, re-expression experiments of Rcan1 in VSMC (present study) and overexpression of Rcan1 in human vein endothelial cells (53) induced a significant decrease in COX-2 expression. Importantly, the increased COX-2 expression induced by *Rcan1* deletion was responsible for the increased phenylephrine contraction observed in aorta from *Rcan1*$^{-/-}$ mice, as shown by the inhibitory effect of the COX-2 inhibitor etoricoxib on vascular contraction, only observed in *Rcan1*$^{-/-}$ mice. The COX-2-derived prostanoid responsible for the increased vascular contraction was probably TXA_2 because both TXAS inhibition with furegrelate and TP blockade with SQ29548 inhibited phenylephrine responses only in *Rcan1*$^{-/-}$ mice. Moreover, increased vascular TXA_2 production was observed in these mice. This excessive TXA_2 might also counterbalance the vasodilator effects of NO. Of note, although little evidence exist that in healthy

conditions COX-2 produces TXA_2, in pathological conditions associated with increased inflammation, increased COX-2 and TXA_2 production have been described [7, 54]. Specifically, COX-2-derived TXA_2 seems to be involved in vascular hypercontractility in spontaneously hypertensive rats [5, 55]. All together, these results demonstrate that at vascular level Rcan1 is an endogenous negative modulator of COX-2 expression and activity and this maintains normal vessel contractility.

Several evidence demonstrate the critical role of COX-2-derived prostanoids in vascular remodelling and vessel stiffness in diverse pathological conditions [12, 13, 56, 57]. Specifically, we have shown that increased COX-2 expression is associated with increased vascular stiffness and that genetic or pharmacological COX-2 blockade restore normal vascular mechanical properties [13]. Our data demonstrate that *Rcan1* deletion differently affect vascular structure in aorta and resistance arteries. Thus, wall thickness remained unaltered in MRA but diminished in aorta from *Rcan1*$^{-/-}$ mice. This aortic hypotrophy might have mechanical consequences [58] and help to explain why vascular stiffness (determined by the relationship between passive tension and diameter) was similar in arteries from both genotypes despite of the presence of more collagen deposition. Interestingly, MRA from *Rcan1*$^{-/-}$ mice exhibit increased vascular stiffness in the absence of altered vessel geometry, which is likely associated to altered elastin structure within the internal elastic lamina as we have demonstrated before [48]. Of note, rofecoxib treatment did not modify vessel structure in aorta or in MRA but it significantly improved vessel elasticity in both vessel types and it normalized collagen deposition but not elastin alterations, suggesting that Rcan1 is an endogenous modulator of normal vessel mechanical properties through the COX-2 pathway.

It is well known that different transcription factors such as CREB, NFAT or NF-κB are involved in the regulation of COX-2 expression in different cell types such as astrocytes, VSMC, epithelial and endothelial cells [26, 28, 29, 32]. Moreover, a relationship between NFAT and NF-κB in the control of COX-2 has been described [32]. Earlier studies identified Rcan1 as a negative regulator of Cn activity [44] and most evidence support these findings in inflammatory situations. However, other evidence suggests that Rcan1 can also act as a facilitator for Cn activity [34, 35] and we recently demonstrated that at vascular level, Rcan1 deletion does not affect Cn activity neither in basal situation nor in response to angiotensin II [36]. Here we demonstrate that the Cn pathway is involved in

the increased participation of COX-2-derived prostanoids in phenylephrine responses observed in aorta from *Rcan1*$^{-/-}$ mice, since the Cn inhibitor CsA, inhibited phenylphrine contractile response and no further effect was observed after CsA and etoricoxib coincubation. On the other hand, Rcan1 regulates NF-κB activity through mechanisms involving the stabilization of the IκB-NF-κB complex [38, 43]. Thus, *Rcan*1 deficiency has been associated to the increase in NF-κB signaling pathway in lung, lymphoma and in mast cells [39-41]. Consistent with this, we found higher levels of phosphorylated-p65 protein and *Il-6* in *Rcan1*$^{-/-}$ aortas and VSMCs. In addition, parthenolide inhibited phenylephrine-contractile responses only in *Rcan1*$^{-/-}$ aortas and no further effect was observed by parthenolide and etoricoxib coincubation, suggesting that Rcan1 is a negative modulator of NF-κB at vascular level.

In conclusion, our results uncover a new role for Rcan1 in vascular contractility and mechanical properties. We describe a basal proinflammatory vascular profile of Rcan1 deficient mice with an activated calcineurin and NF-κB pathways, increased cytokine levels and COX-2 expression and activity that lead to greater vascular contractile responses and increased vascular stiffness. Our results suggest that Rcan1 might act as endogenous negative modulator of COX-2 expression by inhibiting calcineurin and NF-kB pathways to maintain normal vascular stiffness and contractility (Fig. 7).

References

1. Ohnaka K, Numaguchi K, Yamakawa T, Inagami T, Induction of cyclooxygenase-2 by angiotensin II in cultured rat vascular smooth muscle cells, Hypertension 35 (2000) 68-75.

2. Álvarez Y, Pérez-Girón JV, Hernanz R, Briones AM, García-Redondo A, Beltrán A, *et al,* Losartan reduces the increased participation of cyclooxygenase-2-derived products in vascular responses of hypertensive rats, J Pharmacol Exp Ther 321 (2007) 381-388.

3. Montezano AC, Amiri F, Tostes RC, Touyz RM, Schiffrin EL, Inhibitory effects of PPAR-gamma on endothelin-1-induced inflammatory pathways in vascular smooth muscle cells from normotensive and hypertensive rats, J Am Soc Hypertens 1 (2007) 150-160.

4. Martín A, Pérez-Girón JV, Hernanz R, Palacios R, Briones AM, Fortuño A, *et al*., Peroxisome proliferator-activated receptor-γ activation reduces cyclooxygenase-2 expression in vascular smooth muscle cells from hypertensive rats by interfering with oxidative stress, J Hypertens 30 (2012) 315-326.

5. Félétou M, Huang Y, Vanhoutte PM, Endothelium-mediated control of vascular tone: COX-1 and COX-2 products, Br J Pharmacol 164 (2011) 894-912.

6. Hernanz R, Briones AM, Salaices M, Alonso MJ, New roles for old pathways? A circuitous relationship between reactive oxygen species and cyclo-oxygenase in hypertension, Clin Sci (Lond) 126 (2014) 111-121.

7. Ozen G, Norel X, Prostanoids in the pathophysiology of human coronary artery, Prostaglandins Other Lipid Mediat doi: 10.1016/j.prostaglandins.2017.03.003.

8. Adeagbo AS, Zhang X, Patel D, Joshua IG, Wang Y, Sun X, *et al*., Cyclo-oxygenase-2, endothelium and aortic reactivity during deoxycorticosterone acetate salt induced hypertension, J Hypertens. 23 (2005) 1025–1036.

9. Álvarez Y, Briones AM, Balfagón G, Alonso MJ, Salaices M, Hypertension increases the participation of vasoconstrictor prostanoids from cyclooxygenase-2 in phenylephrine responses, J Hypertens. 23 (2005) 767-777.

10. Virdis A, Colucci R, Versari D, Ghisu N, Fornai M, Antonioli L, *et al.,* Atorvastatin prevents endothelial dysfunction in mesenteric arteries from spontaneously hypertensive rats: role of cyclooxygenase 2-derived contracting prostanoids, Hypertension 53 (2009) 1008–1016.

11. Tian XY, Wong WT, Leung FP, Zhang Y, Wang YX, Lee HK, *et al.* Oxidative stress-dependent cyclooxygenase-2-derived prostaglandin f(2α) impairs endothelial function in renovascular hypertensive rats. Antioxid Redox Signal. 16 (2012) 363-373.

12. Martínez-Revelles S, Avendaño MS, García-Redondo AB, Álvarez Y, Aguado A, Pérez-Girón JV, et *al.,* Reciprocal relationship between reactive oxygen species and cyclooxygenase-2 and vascular dysfunction in hypertension. Antioxid Redox Signal. 18 (2013) 51-65.

13. Avendaño MS, Martínez-Revelles S, Aguado A, Simões MR, González-Amor M, Palacios R, *et al.,* Role of COX-2-derived PGE_2 on vascular stiffness and function in hypertension, Br J Pharmacol 173 (2016) 1541-1555.

14. Widlansky ME, Price DT, Gokce N, Eberhardt RT, Duffy SJ, Holbrook M, *et al,* Short- and long-term COX-2 inhibition reverses endothelial dysfunction in patients with hypertension, Hypertension 42 (2003) 310-315.

15. Virdis A, Bacca A, Colucci R, Duranti E, Fornai M, Materazzi G, *et al.,* Endothelial dysfunction in small arteries of essential hypertensive patients: role of cyclooxygenase-2 in oxidative stress generation, Hypertension 62 (2013) 337-344.

16. Crabtree GR, Generic signals and specific outcomes: Signalling through Ca2+, calcineurin and NFAT, Cell 96 (1999) 611-614.

17. Hogan PG, Chen L, Nardone J, Rao A, Transcriptional regulation by calcium, calcineurin, and NFAT, Genes Dev. 17 (2003) 2205-2232.

18. Armesilla AL, Lorenzo E, Gomez del Arco P, Martinez-Martinez S, Alfranca A, Redondo JM, Vascular endothelial growth factor activates nuclear factor of activated T cells in human endothelial cells: a role for tissue factor gene expression, Mol Cell Biol. 19 (1999) 2032-2043.

19. Hill-Eubanks DC, Gomez MF, Stevenson AS, Nelson MT, NFAT regulation in smooth muscle, Trends Cardiovasc Med. 13 (2003) 56-62.

20. Nilsson LM, Nilsson-Ohman J, Zetterqvist AV, Gomez MF, Nuclear factor of activated T-cells transcription factors in the vasculature: the good guys or the bad guys?, Curr Opin Lipidol. 19 (2008) 483-490.

21. Coffman TM, Carr DR, Yarger WE, Klotman PE, Evidence that renal prostaglandins and thromboxane production is stimulated in chronic cyclosporine nephrotoxicity. Transplantation 43 (1987) 282–285.

22. Kiani A, Rao A, Aramburu J, Manipulating immune responses with immunosuppressive agents that target NFAT, Immunity 12 (2000) 359-72.

23. Martínez-Martínez S, Redondo JM, Inhibitors of the calcineurin/NFAT pathway, Curr Med Chem. 8 (2004) 997-1007.

24. Kou R, Greif D, Michel T, Dephosphorylation of Endothelial Nitric Oxide Synthase by Vascular Endothelial Growth Factor: Implications for the Vascular Responses to Cyclosporin A, J Biol Chem 277 (2002) 29669–29673.

25. Ruan L, Torres CM, Buffett RJ, Kennard S, Fulton D, Venema RC, Calcineurin-mediated dephosphorylation of eNOS at serine 116 affects eNOS enzymatic activity indirectly by facilitating c-Src binding and tyrosine 83 phosphorylation, Vasc Pharmacol 59 (2013) 27-35.

26. Robida AM, Xu K, Ellington ML, Murphy TJ, Cyclosporin A selectively inhibits mitogen-induced cyclooxygenase-2 gene transcription in vascular smooth muscle cells, Mol Pharmacol 58 (2000) 701-8.

27. Hernández GL, Volpert OV, Iñiguez MA, Lorenzo E, Martínez-Martínez S, Grau R, *et al.,* Selective inhibition of vascular endothelial growth factor-mediated angiogenesis by cyclosporin A: roles of the nuclear factor of activated T cells and cyclooxygenase 2, J Exp Med 193 (2001) 607-620.

28. Canellada A, Ramirez BG, Minami T, Redondo JM, Cano E, Calcium/calcineurin signaling in primary cortical astrocyte cultures: Rcan1-4 and cyclooxygenase-2 as NFAT target genes, Glia 56 (2008) 709-722.

29. Sharma-Walia N, George Paul A, Patel K, Chandran K, Ahmad W, Chandran B, NFAT and CREB regulate Kaposi's sarcoma-associated herpesvirus-induced cyclooxygenase 2 (COX-2), J Virol. 84 (2010) 12733-12753.

30. Pérez-Girón JV, Palacios R, Martín A, Hernanz R, Aguado A, Martínez-Revelles S, *et al.,* Pioglitazone reduces angiotensin II-induced COX-2 expression through the inhibition of ROS production and ET-1 transcription in vascular cells from SHR rats, Am J Physiol Heart Circ Physiol. 306 (2014) H1582-593.

31. Williams CR, Gooch J, Calcineurin Aβ regulates NADPH oxidase (Nox) expression and activity via nuclear factor of activated T cells (NFAT) in response to high glucose, J Biol Chem. 289 (2014) 4896-4905.

32. Cai T, Li X, Ding J, Luo W, Li J, Huang C, A cross-talk between NFAT and NF-κB pathways is crucial for nickel-induced COX-2 expression in Beas-2B cells, Curr Cancer Drug Targets 11 (2011) 548-559.

33. Rothermel B, Vega RB, Yang J, Wu H, Bassel-Duby R, Williams RS, A protein encoded within the Down syndrome critical region is enriched in striated muscles and inhibits calcineurin signaling, J Biol Chem. 275 (2000) 8719-8725.

34. Kingsbury TJ, Cunningham KW, A conserved family of calcineurin regulators. Genes Dev. 14 (2000) 1595-15604.

35. Vega RB, Rothermel BA, Weinheimer CJ, Kovacs A, Naseem RH, Bassel-Duby R, *et al*., Dual roles of modulatory calcineurin-interacting protein 1 in cardiac hypertrophy, Proc Natl Acad Sci USA. 100 (2003) 669–674.

36. Esteban V, Méndez-Barbero N, Jiménez-Borreguero LJ, Roqué M, Novensá L, García-Redondo AB, *et al.,* Regulator of calcineurin 1 mediates pathological vascular wall remodeling. J Exp Med. 208 (2011) 2125-21395.

37. Méndez-Barbero N, Esteban V, Villahoz S, Escolano A, Urso K, Alfranca A, *et al.,* A major role for RCAN1 in atherosclerosis progression, EMBO Mol Med. 5 (2013) 1901-1917.

38. Kim YS, Cho KO, Lee HJ, Kim SY, Sato Y, Cho YJ, Down syndrome candidate region 1 increases the stability of the IkappaBalpha protein: implications for its anti-inflammatory effects, J Biol Chem. 281 (2006) 39051-39061.

39. Junkins RD, Macneil AJ, Wu Z, McCormick C, Lin TJ, Regulator of Calcineurin 1 Suppresses Inflammation during Respiratory Tract Infections, J Immunol. 190 (2013) 5178-5186.

40. Wu Z, Li Y, MacNeil AJ, Junkins RD, Berman JN, Lin TJ, Calcineurin-Rcan1 interaction contributes to stem cell factor-mediated mast cell activation, J Immunol. 191 (2013) 5885-5894.

41. Liu C, Zheng L, Wang H, Ran X, Liu H, Sun X, The RCAN1 inhibits NF-κB and suppresses lymphoma growth in mice, Cell Death Dis. 6 (2015) e1929.

42. Minami T, Yano K, Miura M, Kobayashi M, Suehiro J, Reid PC, *et al,* The Down syndrome critical region gene 1 short variant promoters direct vascular bed-specific gene expression during inflammation in mice, J Clin Invest. 119 (2009) 2257–2270.

43. Yang YJ, Chen W, Edgar A, Li B, Molkentin JD, Berman JN, *et al.,* Rcan1 negatively regulates Fc epsilonRI-mediated signalling and mast cell function, J Exp Med. 206 (2009) 195–207.

44. Rothermel BA, McKinsey TA, Vega RB, Nicol RL, Mammen P, Yang J*, et al.,* Myocyte-enriched calcineurin-interacting protein, MCIP1, inhibits cardiac hypertrophy in vivo, Proc Natl Acad Sci USA. 98 (2001) 3328–3333.

45. Kilkenny C, Browne W, Cuthill IC, Emerson M, Altman DG, Animal research: reporting in vivo experiments: the ARRIVE guidelines, Br J Pharmacol. 160 (2010) 1577-9.

46. Porta S, Serra SA, Huch M, Valverde MA, Llorens F, Estivill X, *et al.,* RCAN1 (DSCR1) increases neuronal susceptibility to oxidative stress: a potential pathogenic process in neurodegeneration, Hum Mol Genet. 16 (2007) 1039–1050.

47. Kingwell BA, Arnold PJ, Jennings GL, Dart AM, Spontaneous running increases aortic compliance in Wistar-Kyoto rats, Cardiovasc Res. 35 (1997) 132–137.

48. Briones AM, González JM, Somoza B, Giraldo J, Daly CJ, Vila E, *et al.,* Role of elastin in spontaneously hypertensive rat small mesenteric artery remodelling, J Physiol 552 (2003) 185-195.

49. Minami T, Horiuchi K, Miura M, Abid MR, Takabe W, Noguchi N, *et al.,* Vascular endothelial growth factor- and thrombin-induced termination factor, Down syndrome critical region-1, attenuates endothelial cell proliferation and angiogenesis, J Biol Chem 279 (2004) 50537-50554.

50. Holmes K, Chapman E, See V, Cross MJ, VEGF stimulates RCAN1.4 expression in endothelial cells via a pathway requiring Ca2+/calcineurin and protein kinase C-delta, PLoS One 5 (2010) e11435.

51. Riper DV, Jayakumar L, Latchana N, Bhoiwala D, Mitchell AN, Valenti JW, *et al.,* Regulation of vascular function by RCAN1 (ADAPT78), Arch Biochem Biophys 472 (2008) 43-50.

52. Sobrado M, Ramirez BG, Neria F, Lizasoain I, Arbones ML, Minami T, *et al.,* Regulator of calcineurin 1 (Rcan1) has a protective role in brain ischemia/reperfusion injury, J Neuroinflammation 9 (2012) 48.

53. Ballesteros-Martinez C, Mendez-Barbero N, Montalvo-Yuste A, M Jensen B, Gomez-Cardenosa A, Klitfod L, Garrido-Arandia M, *et al*. Endothelial regulator of calcineurin 1 (Rcan1) promotes barrier integrity and modulates histamine-induced barrier dysfunction in anaphylaxis. Front. Immunol. | doi: 10.3389/fimmu.2017.01323. In press

54. Huang QC, Huang RY, The cyclooxygenase-2/thromboxane A2 pathway: a bridge from rheumatoid arthritis to lung cancer?, Cancer Lett. 354 (2014) 28-32.

55. D'Abril Ruíz-Leyja E, Villalobos-Molina R, López-Guerrero JJ, Gallardo-Ortíz IA, Estrada-Soto SE, Ibarra-Barajas M, Differential role of cyclooxygenase-1 and -2 on renal vasoconstriction to α_1-adrenoceptor stimulation in normotensive and hypertensive rats, Life Sci. 93 (2013) 552-557.

56. Gitlin JM, Trivedi DB, Langenbach R, Loftin CD, Genetic deficiency of cyclooxygenase-2 attenuates abdominal aortic aneurysm formation in mice, Cardiovasc Res 73 (2007) 227-236.

57. Zhang J, Zou F, Tang J, Zhang Q, Gong Y, Wang Q, *et al.,* Cyclooxygenase-2-derived prostaglandin E_2 promotes injury-induced vascular neointimal hyperplasia through the E-prostanoid 3 receptor, Circ Res. 113 (2013) 104-114.

58. van den Akker J, Schoorl MJ, Bakker EN, Vanbavel E, Small artery remodeling: current concepts and questions, J Vasc Res. 47 (2010) 183-202.

Acknowledgements

This study was supported by Ministerio de Economía y Competitividad (MINECO, SAF2012-36400 and SAF2016-80305-P), Instituto de Salud Carlos III (ISCIII) (Red de Investigación Cardiovascular, RD12/0042/0022 and RD12/0042/0024, CiberCV CB16/11/00286 and CB16/11/00264 and PI13/01488), Fondo Europeo de Desarrollo Regional (FEDER) a way to

build Europe, COST BM1301 and Roche-IdiPaz. VE was supported by the Ramón y Cajal Program (RYC-2013-12880).

Author Contributions Statement

ABG-R, VE, LSDdelC and NM-B contributed to performance the experimental work; ABG-R and VE to writing the original draft; AMB, MS, MRC and JMR to writing, review & editing.

Conflict of interest

Authors declare no competing financial interests.

Declarations of transparency and scientific rigour

This Declaration acknowledges that this paper adheres to the principles for transparent reporting and scientific rigour of preclinical research recommended by funding agencies, publishers and other organizations engaged with supporting research.

Figure Legends

Figure 1. Rcan1 modulates aortic vascular contraction. Vascular responses to acetylcholine (ACh, A), and phenylephrine (Phe, B) in aortic segments from *Rcan1*$^{+/+}$ (n=16) and *Rcan1*$^{-/-}$ (n=14) mice. (C) mRNA levels of α1A-adrenoceptors (Adr1a) in aorta from *Rcan1*$^{+/+}$ (n=12) and *Rcan1*$^{-/-}$ (n=12) mice. (D) Concentration–response curves to phenylephrine-induced contraction in intact and endothelium-denuded (E-) aortic segments from *Rcan1*$^{+/+}$ (n=6) and *Rcan1*$^{-/-}$ (n=6) mice. (E) Effect of L-NAME (100 μM) or tiron (1 mM) on vasoconstrictor responses to phenylephrine (n=5-6). (F) eNOS and pAkt immunoblots (left panel) and quantification (right panels) in homogenates of aorta from *Rcan1*$^{+/+}$ (n=6) and *Rcan1*$^{-/-}$ mice (n=8). β-actin was used as loading control. Data are expressed as mean ± s.e.m. *$p<0.05$ *vs* control or *Rcan1*$^{+/+}$ mice.

Figure 2. Rcan1 modulates vascular COX-2 expression. (A) Representative COX-2 immunofluorescence of aortic sections from *Rcan1*$^{+/+}$ (n=5) and *Rcan1*$^{-/-}$ (n=5) mice; negative control is also shown. Image size: 375 x 375 μm. Arrows point to endothelial cells (EC), vascular smooth muscle cells (VSMC) and adventitial cells (AC). qPCR

analysis of *Cox-2* mRNA levels in aorta or VSMC (B,D) derived from *Rcan1*$^{+/+}$ (n=8) and *Rcan1*$^{-/-}$ (n=9) mice. COX-2 immunoblot (upper panel) and quantification (bottom panel) in extracts from aorta (C) or VSMC (E) derived from *Rcan1*$^{+/+}$ (n=5) and *Rcan1*$^{-/-}$ mice (n=6). β-actin or tubulin was used as loading control in aortic homogenates or VSMC, respectively. (F) COX-2 immunoblot (upper panel) and quantification (bottom panel) in extracts from VSMC derived from *Rcan1*$^{+/+}$ and *Rcan1*$^{-/-}$ mice infected with adenovirus encoding GFP-RCAN1-4 (Ad-RCAN1) or empty GFP-adenovirus (Ad-GFP). β-actin was detected as a loading control. Representative experiments are shown of nine performed. Gene and protein data are expressed as fold increase of the control group mean value. Data are expressed as mean ± s.e.m. *p< 0.05 *vs* *Rcan1*$^{+/+}$; $^{\#}$p<0.05 *vs* *Rcan1*$^{-/-}$.

Figure 3. Rcan1 modulates COX-2 participation on vascular contractility. Effect of etoricoxib (1 μM), furegrelate (100 μM) and SQ 29548 (1 μM) on the concentration–response curve to phenylephrine in intact aortic segments from *Rcan1*$^{+/+}$ (n= 8-16) and *Rcan1*$^{-/-}$ (n=8-14) mice (A,B). TXB_2 production (C) and TXA synthase (TXAS) protein expression (D) in aorta from *Rcan1*$^{+/+}$ (n=6) and *Rcan1*$^{-/-}$ (n=6) mice. Data are expressed as mean ± s.e.m. *p<0.05 *vs* control or *Rcan1*$^{+/+}$ mice.

Figure 4. Rcan1 modulates NF-kB activation. (A) Representative phospho-p65 (pp65) immunoblot (upper panel) and quantification (bottom panels) in VSMC from *Rcan1*$^{+/+}$ (n=6) and *Rcan1*$^{-/-}$ mice (n=8). β-actin was detected as a loading control. (B) Representative pp65 immunostaining and quantification of paraffin-embedded aortic sections from *Rcan1*$^{+/+}$ (n=5) and *Rcan1*$^{-/-}$ (n=5) mice. (C) mRNA expression of *Il-6* in aorta and VSMC from *Rcan1*$^{+/+}$ (n=5-7) and *Rcan1*$^{-/-}$ (n=5-8). Gene and protein data are expressed as fold increase of the control group mean value. (D and E) Effect of cyclosporine A (CsA, 200 ng/ml) or parthenolide (1 μM) in the absence or in the presence of etoricoxib (1 μM) on the concentration–response curve to phenylephrine in aortic segments from *Rcan1*$^{+/+}$ (n=6-8) and *Rcan1*$^{-/-}$ (n=6-8) mice. Data are expressed as mean ± s.e.m. *p<0.05 *vs* control or *Rcan1*$^{+/+}$ mice.

Figure 5. Rcan1 modulates vascular structural properties. (A) Vessel and lumen diameter, wall:lumen ratio, wall thickness and cross sectional area (CSA) of mesenteric resistance arteries (MRA) from *Rcan1*$^{+/+}$ (n=12), *Rcan1*$^{-/-}$ (n=11), and *Rcan1*$^{-/-}$ mice treated with rofecoxib (n=6). (B) Media thickness and CSA of aorta from *Rcan1*$^{+/+}$ (n=7), *Rcan1*$^{-/-}$ (n=9) and *Rcan1*$^{-/-}$ mice treated with rofecoxib (n=6). Representative images of

hematoxylin-eosin stained aortic sections from all groups of mice are also shown. x60. Results are expressed as mean ± s.e.m. *p<0.05 *vs* *Rcan1*$^{+/+}$ mice.

Figure 6. Rcan1 modulates vascular mechanical properties. (A) Mechanical parameters (stress-strain curve and β values) of mesenteric resistance arteries (MRA) from *Rcan1*$^{+/+}$ (n=12), *Rcan1*$^{-/-}$ (n=11), and *Rcan1*$^{-/-}$ mice treated with rofecoxib (n=6) (B) Representative images and quantification of internal elastic lamina structure of MRA (n = 6–9). Image size: 93.75 x 93.75 μm (x40, zoom 4). (C) Tension-extension distance relationship and 1/slope of this relationship in aorta from *Rcan1*$^{+/+}$ (n=10), *Rcan1*$^{-/-}$ (n=12), and *Rcan1*$^{-/-}$ mice treated with rofecoxib (n=6). (D) mRNA level of collagen 1a2 (*Col1a2*) and fibronectin (*Fn1*) in aortic homogenates from *Rcan1*$^{+/+}$ (n=11), *Rcan1*$^{-/-}$ (n=9), and *Rcan1*$^{-/-}$ mice treated with rofecoxib (n=6). Gene data are expressed as fold increase of the control group mean value. Results are expressed as mean ± s.e.m. *p<0.05 *vs* *Rcan1*$^{+/+}$ mice; $^{\#}$p<0.05 *vs* *Rcan1*$^{-/-}$.

Figure 7. Rcan1 modulation of vascular tone and stiffness. Vascular tone and stiffness are modulated, among others, by nitric oxide (NO), reactive oxygen species (ROS) likely derived from NADPH Oxidase (NOX) and prostanoids derived from COX-2. At vascular level, COX-2 expression is regulated by different signalling pathways such as Cn/NFAT and NF-kB. Cn/NFAT signalling pathway is activated by increase in intracellular calcium (Ca^{2+}). Phosphorylation of IkB is required for the canonical activation of NF-kB, IkB-phosphorylated is released from the NF-kB complex, and the p50/p65 subunit translocate to the nucleus. In physiological conditions, Rcan1 acts as negative modulator of Cn/NFAT and NF-kB and prevent the activation of both signalling pathways. Rcan1 deficiency increases Cn-NFAT and NF-kB activities and, therefore, COX-2 expression and TXA_2 and ROS production. In these conditions, an increase in ROS and a decrease in NO bioavailability are produced. All these factors facilitate an increase in vasoconstriction and in the vascular stiffness.

Fig. S1. Vascular responses to acetylcholine (ACh) (A) and phenylephrine (Phe) (B) in mesenteric resistance arteries from *Rcan1*$^{+/+}$ (n=6) and *Rcan1*$^{-/-}$ (n=6) mice. (C) Plasma NOx of *Rcan1*$^{+/+}$ (n=13) and *Rcan1*$^{-/-}$ (n=15). Results are expressed as mean ± s.e.m.

Fig. S2. Original uncropped images of blots shown in Figures 1, 2, 3. Bands in squares correspond to those shown in the Figures.

Fig. S3. (A) Representative COX-2 immunostaining and quantification of paraffin-embedded aortic sections from *Rcan1*$^{+/+}$ (n=7) and *Rcan1*$^{-/-}$ (n=7) mice. (B) Representative COX-1 immunofluorescence of aortic sections from *Rcan1*$^{+/+}$ (n=5) and *Rcan1*$^{-/-}$(n=5) mice; negative control is also shown. Image size: 775 x 775 µm (x20, upper panels) and 387.5 x 387, 5 µm (x40, lower panels). (C) qPCR analysis of *Cox-1* mRNA levels in aorta from *Rcan1*$^{+/+}$ (n=5) and *Rcan1*$^{-/-}$ (n=5) mice. Gene data are expressed as fold increase of the control group mean value. (D) Plasma PGE_2 levels of *Rcan1*$^{+/+}$ (n=10) and *Rcan1*$^{-/-}$ (n=12). Results are expressed as mean ± s.e.m. *$p<0.05$ *vs Rcan1*$^{+/+}$ mice.

Fig. S4. Representative immunofluorescence of colocalization of Calcineurin (Cn), COX-2 and Rcan1 in aortic sections from *Rcan1*$^{+/+}$ (n=5). Arrows point to single cells. Image size: 512 x 512 µm (x40, upper panels) and magnification 200 x 200 µm (bottom panels).

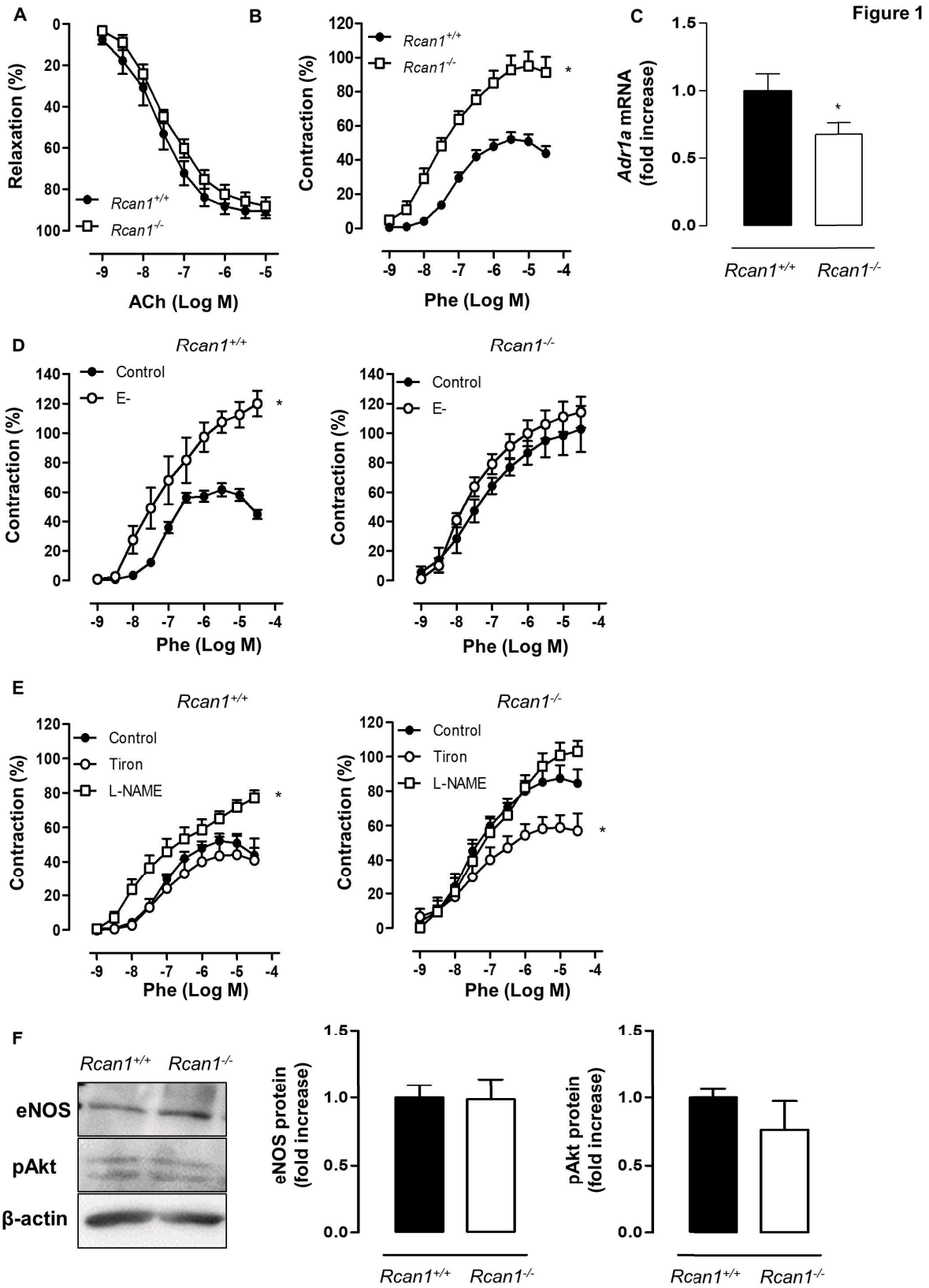
A
Relaxation (%)
Rcan1+/+
Rcan1-/-
ACh (Log M)
B
Contraction (%)
Rcan1+/+
Rcan1-/-
*
Phe (Log M)
C
Adr1a mRNA (fold increase)
*
Rcan1+/+
Rcan1-/-
Figure 1
D
Rcan1+/+
Rcan1-/-
Control
E-
Contraction (%)
Phe (Log M)
E
Rcan1+/+
Rcan1-/-
Control
Tiron
L-NAME
Contraction (%)
Phe (Log M)
F
Rcan1+/+
Rcan1-/-
eNOS
pAkt
β-actin
eNOS protein (fold increase)
pAkt protein (fold increase)
Rcan1+/+
Rcan1-/-

Figure 2

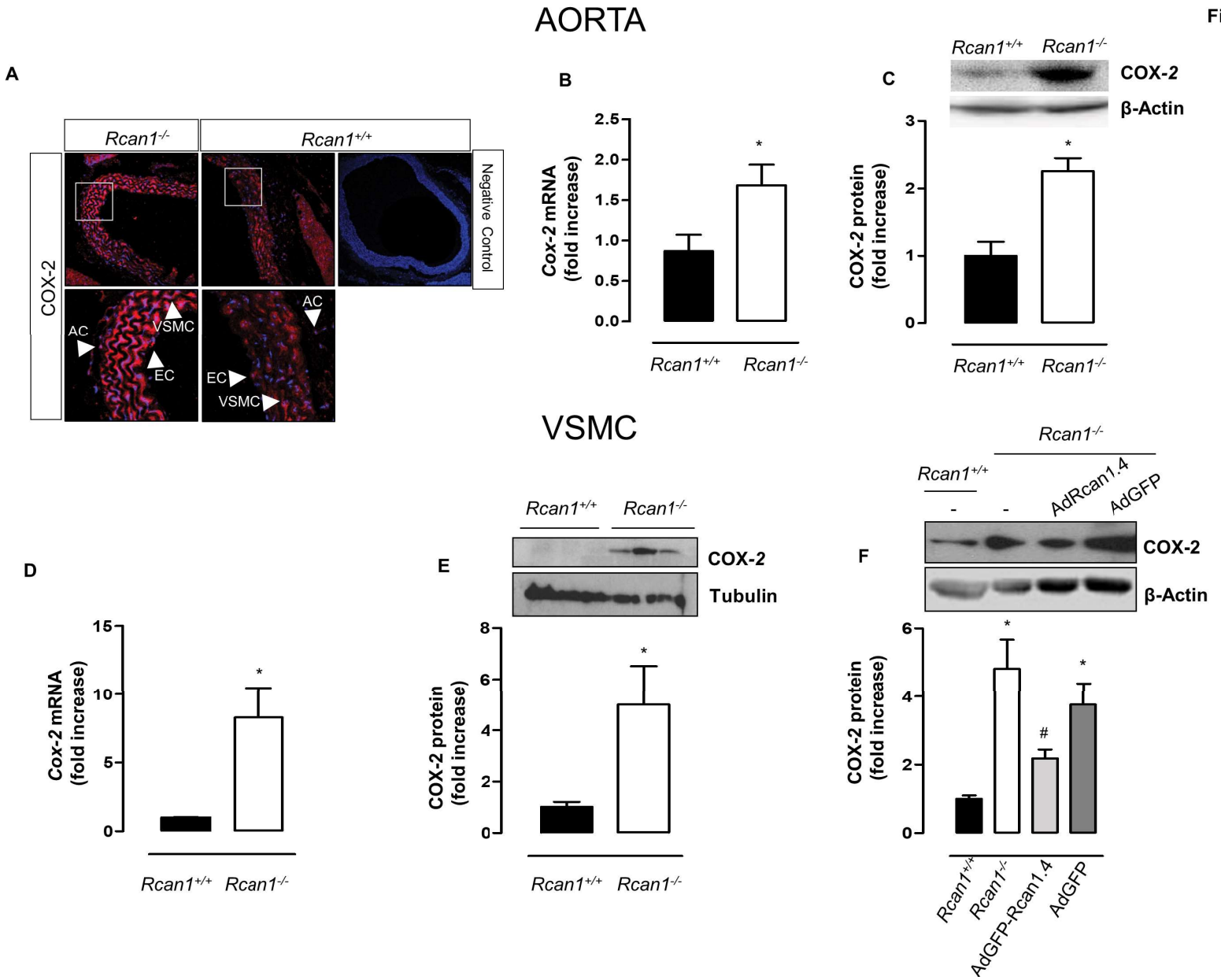
AORTA
A
Rcan1-/-
Rcan1+/+
COX-2
Negative Control
AC
VSMC
EC
B
Cox-2 mRNA (fold increase)
Rcan1+/+
Rcan1-/-
C
COX-2
β-Actin
COX-2 protein (fold increase)
VSMC
D
E
Tubulin
F
AdRcan1.4
AdGFP
AdGFP-Rcan1.4

Figure 3

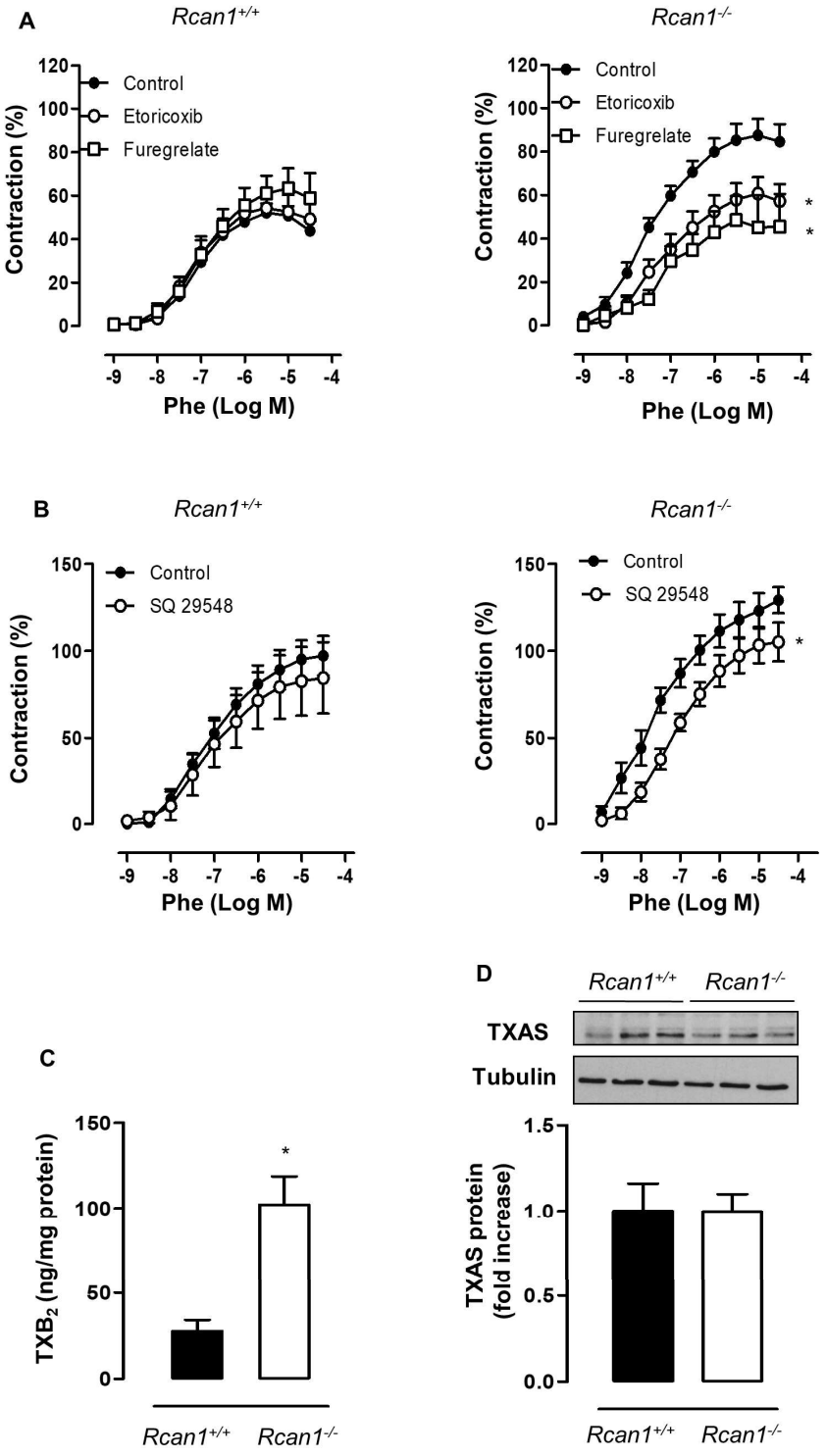
A
Rcan1+/+
Rcan1-/-
Control
Etoricoxib
Furegrelate
Contraction (%)
Phe (Log M)
B
SQ 29548
C
TXB2 (ng/mg protein)
D
TXAS
Tubulin
TXAS protein (fold increase)

Figure 4

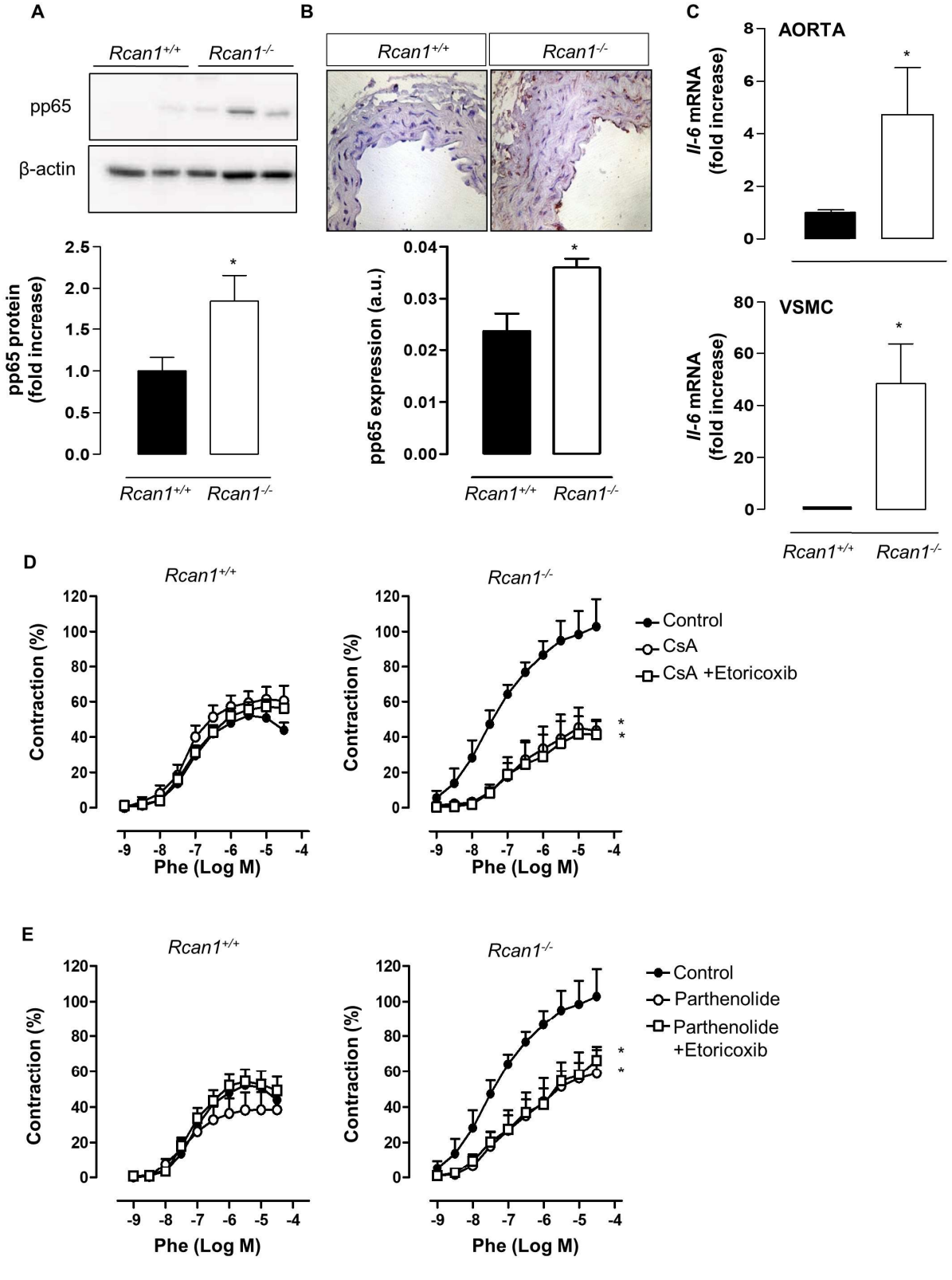
A
Rcan1+/+
Rcan1-/-
pp65
β-actin
pp65 protein (fold increase)
B
pp65 expression (a.u.)
C
AORTA
Il-6 mRNA (fold increase)
VSMC
D
Contraction (%)
Phe (Log M)
Control
CsA
CsA +Etoricoxib
E
Parthenolide
Parthenolide +Etoricoxib

Figure 5

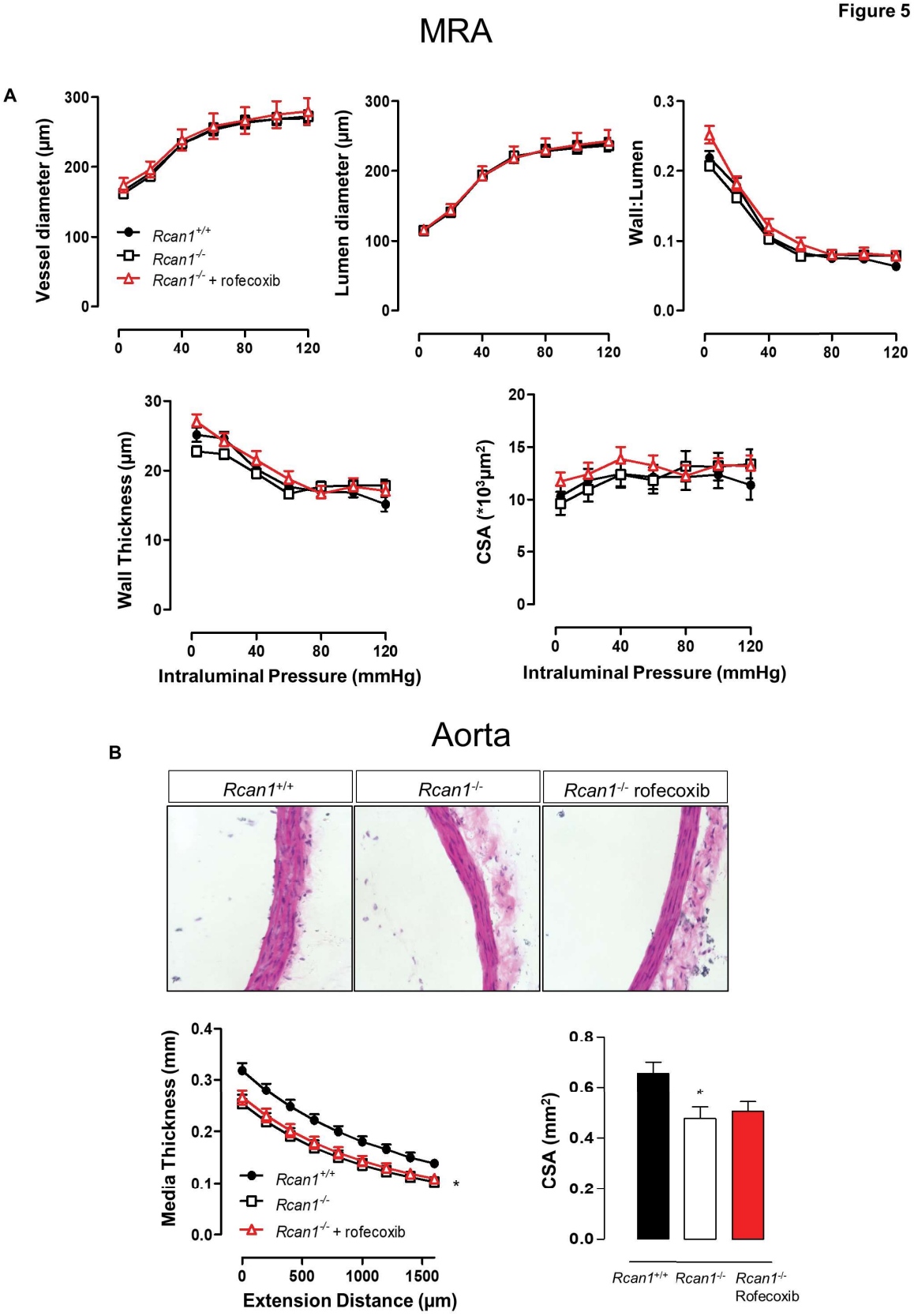
MRA
A
Vessel diameter (µm)
Lumen diameter (µm)
Wall:Lumen
Rcan1+/+
Rcan1-/-
Rcan1-/- + rofecoxib
Wall Thickness (µm)
CSA (*10³µm²)
Intraluminal Pressure (mmHg)
Intraluminal Pressure (mmHg)
Aorta
B
Rcan1+/+
Rcan1-/-
Rcan1-/- rofecoxib
Media Thickness (mm)
Extension Distance (µm)
CSA (mm²)
Rcan1+/+
Rcan1-/-
Rcan1-/-
Rofecoxib

Figure 6

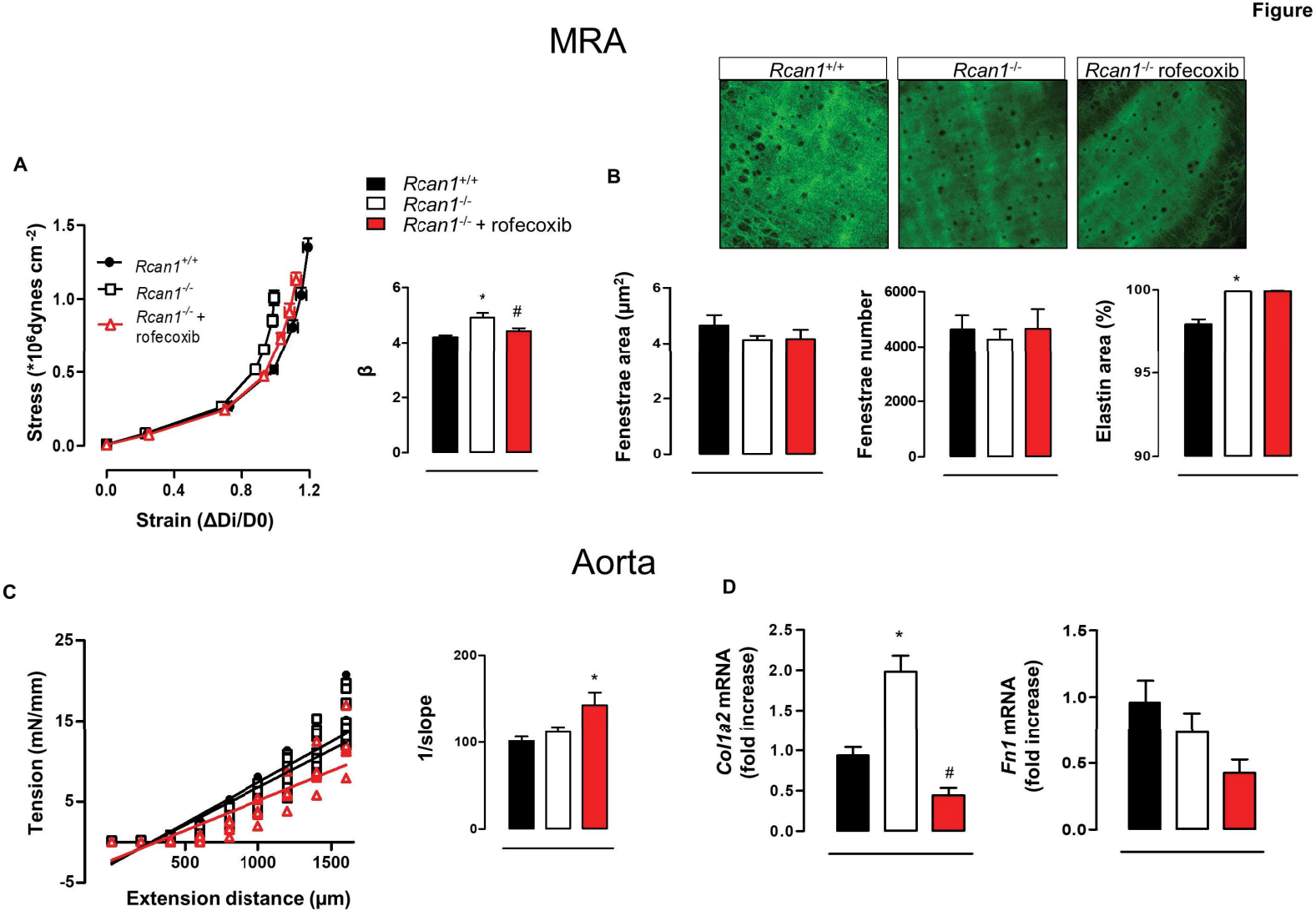
MRA
A
Rcan1+/+
Rcan1-/-
Rcan1-/- + rofecoxib
Stress (*10^6dynes cm^-2)
Strain (ΔDi/D0)
β
B
Rcan1+/+
Rcan1-/-
Rcan1-/- rofecoxib
Fenestrae area (μm²)
Fenestrae number
Elastin area (%)
Aorta
C
Tension (mN/mm)
Extension distance (μm)
1/slope
D
Col1a2 mRNA (fold increase)
Fn1 mRNA (fold increase)

Figure 7

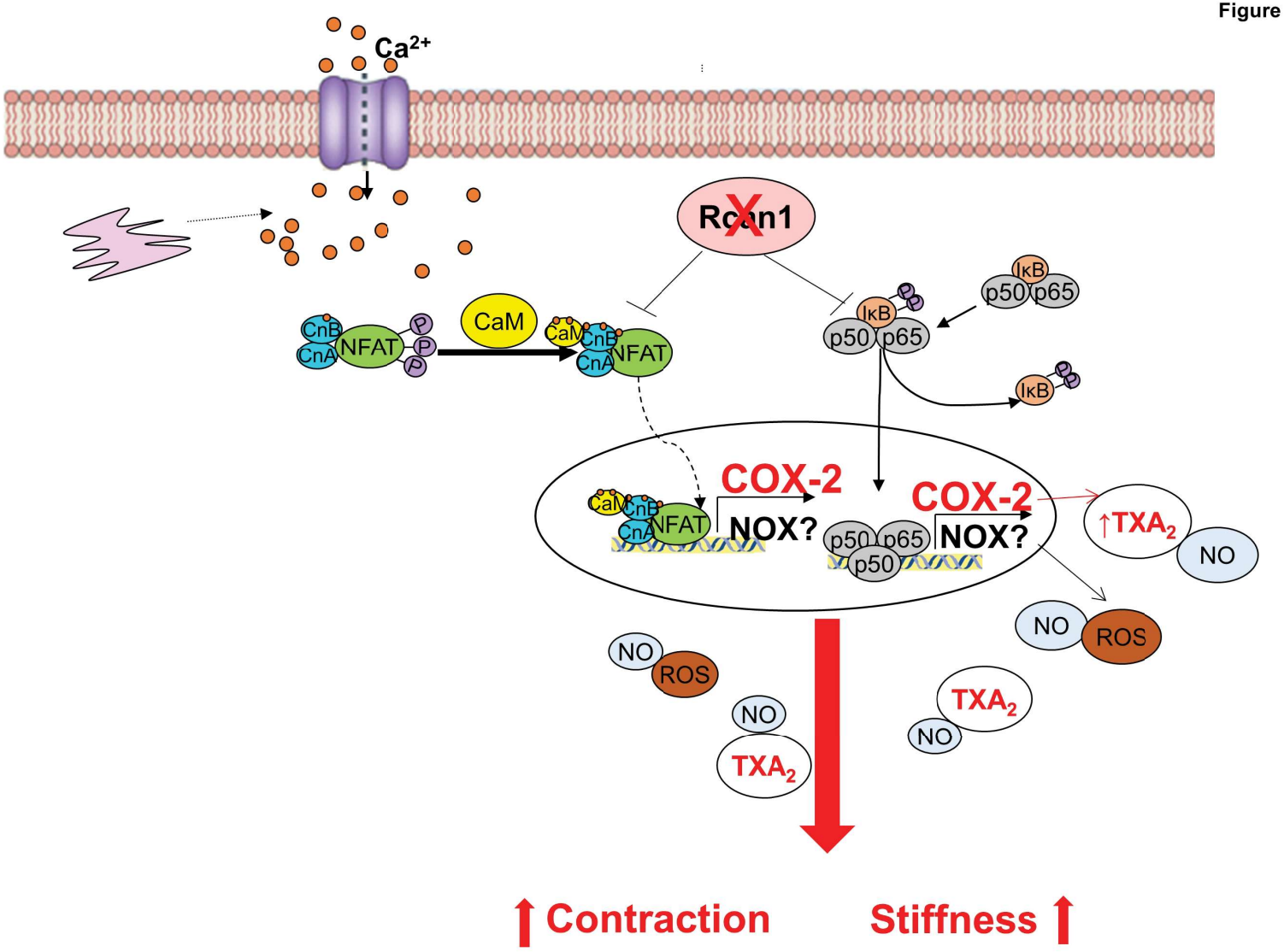
Ca2+
Rcan1
X
CaM
CnB
CnA
NFAT
P
IκB
p50
p65
COX-2
NOX?
↑TXA2
NO
ROS
TXA2
↑ Contraction
Stiffness ↑

Supporting Information Fig. S1

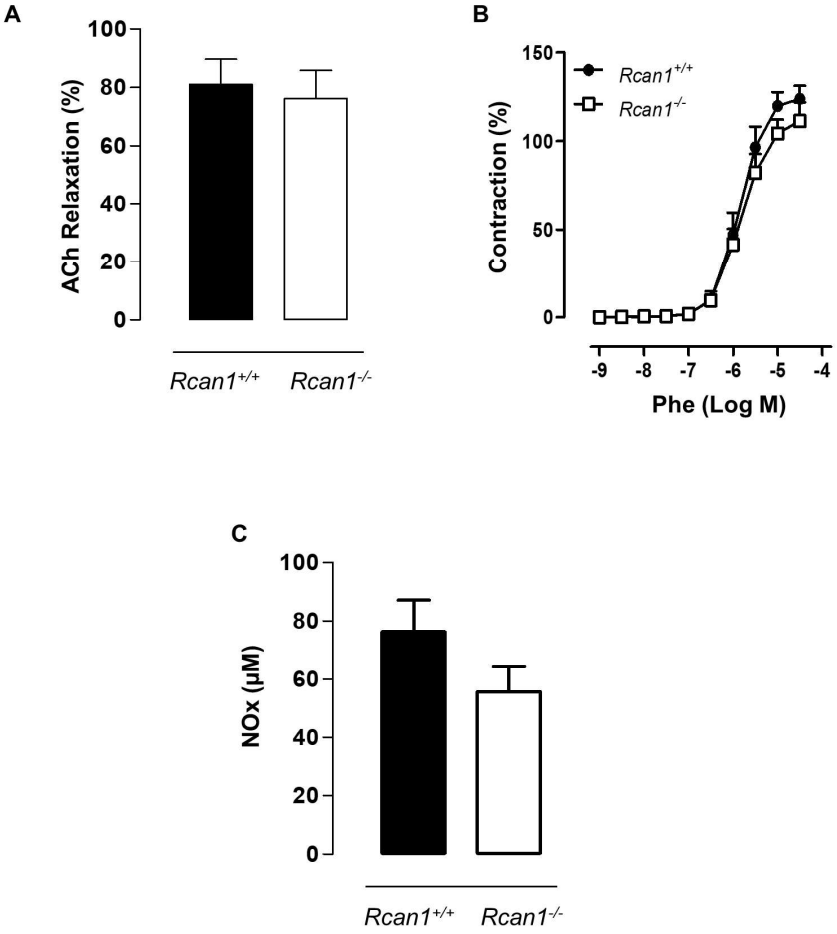

Supporting Information Fig. S2

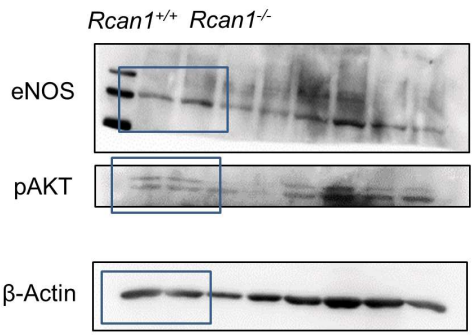

Aorta

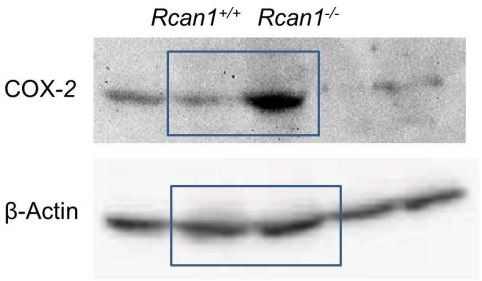

VSMC-AdRcan1.4

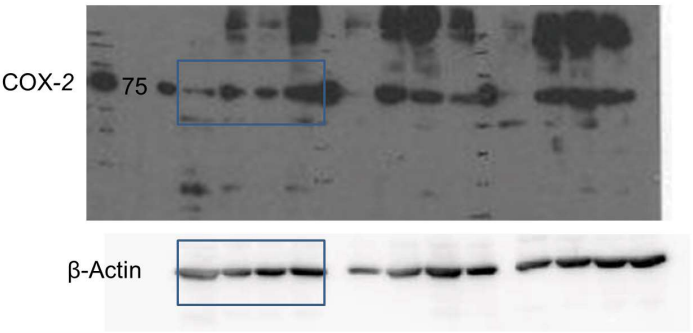

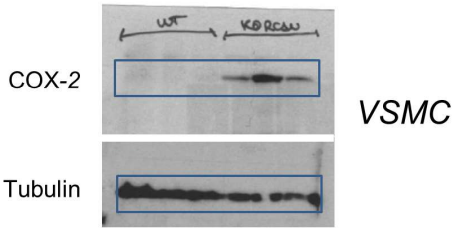

VSMC

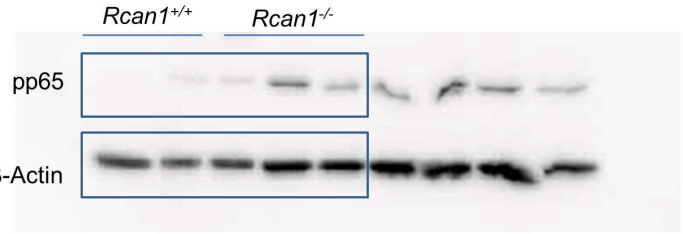

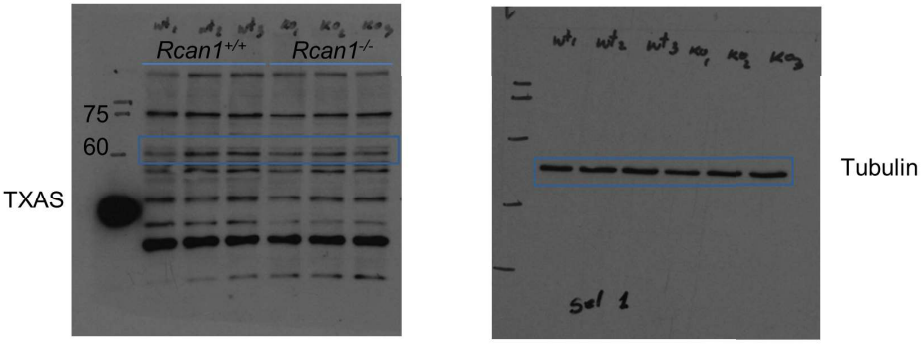

Supporting Information Fig. S3

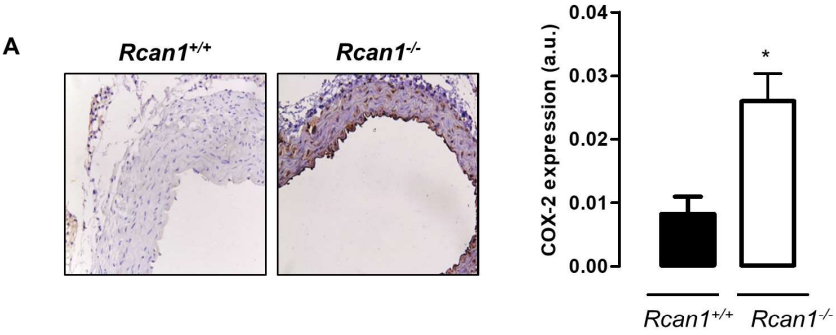

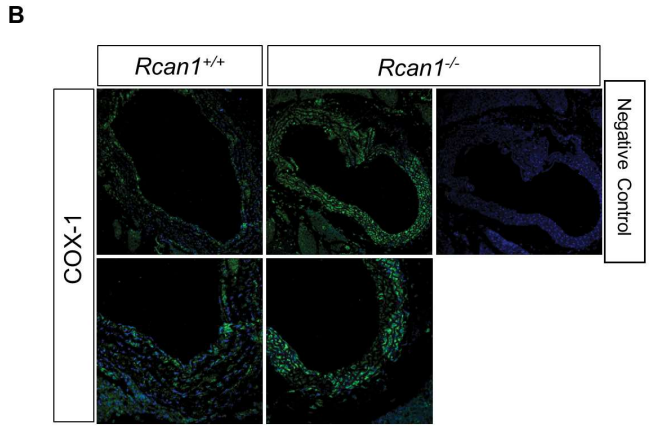

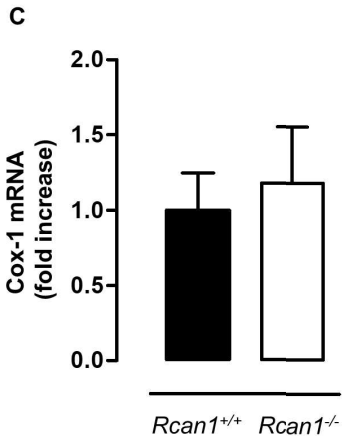

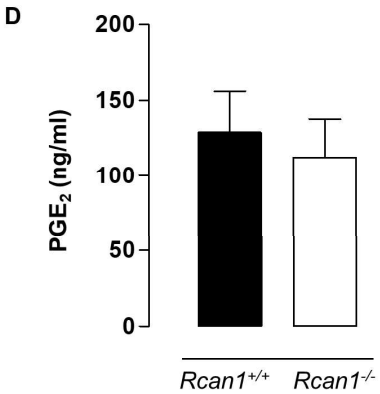

Supporting Information Fig. S4

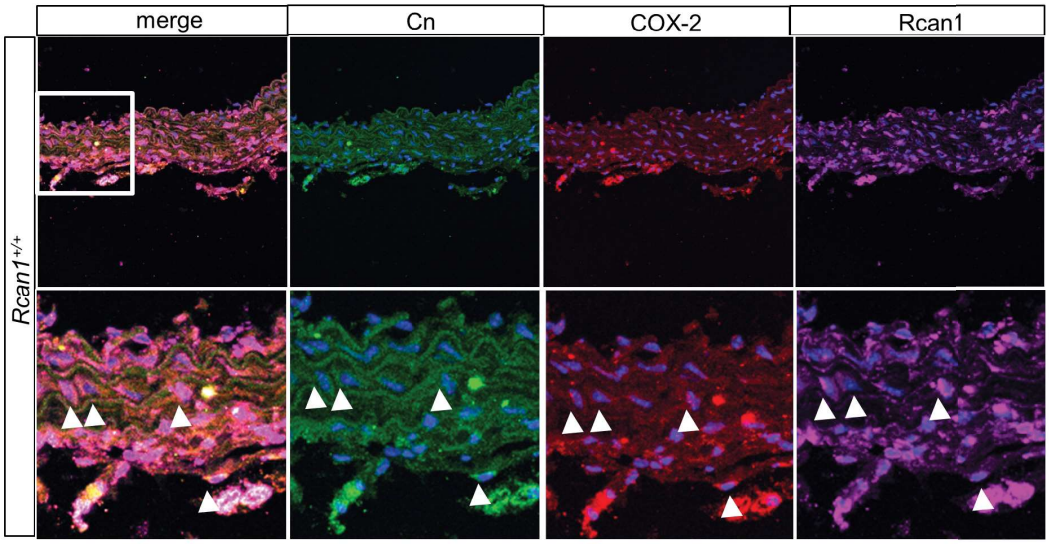

Table 1. Maximal response (Emax) and pD_2 (-logEC50 values) of KCl and phenylephrine (Phe) in aorta and mesenteric resistance arteries (MRA) from *Rcan1*$^{+/+}$ and *Rcan1*$^{-/-}$ mice.

		***Rcan1*$^{+/+}$**		***Rcan1*$^{-/-}$**	
		Emax (mN/mm)	**pD_2**	**Emax (mN/mm)**	**pD_2**
Aorta	**KCl**	2.3 ± 0.2 (16)		1.9 ± 0.2 (15)	
	Phe	1.3 ± 0.2 (16)	7.10±0.05	2.1 ± 0.2 (15)*	8 ± 0.28*
MRA	**KCl**	1.9 ± 0.1 (6)		1.8 ± 0.2 (6)	
	Phe	2.2 ± 0.2 (6)	6.15±0.17	2 ± 0.1 (6)	6.4 ± 0.2

Data are expressed as mean ± SEM of the number of animals indicated in parenthesis. * $p< 0.05$ vs *Rcan1*$^{+/+}$.